

# Late Quaternary subsidence of Santa Catalina Island, California Continental Borderland, demonstrated by seismic-reflection data and fossil assemblages from submerged marine terraces

Chris M. Castillo<sup>1,†</sup>, Simon L. Klemperer<sup>1,§</sup>, James C. Ingle Jr.<sup>1,§</sup>, Charles L. Powell II<sup>2,§</sup>, Mark R. Legg<sup>3,§</sup>, and Robert D. Francis<sup>4,§</sup>

<sup>1</sup>*Department of Geophysics, Stanford University, Mitchell Building, 397 Panama Mall, Stanford, California 94305, USA*

<sup>2</sup>*U.S. Geological Survey, Western Region Geology and Geophysics Science Center, 345 Middlefield Road, Menlo Park, California 94025, USA*

<sup>3</sup>*Legg Geophysical, 16541 Gothard Street, #107, Huntington Beach, California 92647, USA*

<sup>4</sup>*Department of Geological Sciences, California State University–Long Beach, 1250 Bellflower Boulevard, Long Beach, California 90840, USA*

## ABSTRACT

Submerged paleoshorelines and terraces surrounding Santa Catalina Island and the Pilgrim/Kidney Banks in the California Continental Borderland demonstrate late Quaternary tectonic subsidence, in contrast to the other islands of the California Continental Borderland that are experiencing tectonic uplift. We used high-resolution seismic-reflection profiles to map a terrace package containing 16 successive parasequences surrounding Santa Catalina Island, preserved at depths from 30 to 470 m below modern mean sea level. The Pilgrim/Kidney Banks are surrounded by a terrace package containing 13 successive parasequences preserved at 90–310 m depth. The presence of marine terrace (beach) deposits at >400 m depth, far below the lowest estimates of Quaternary lowstand sea level (90–130 m), requires significant tectonic subsidence. Within each terrace, we identified the transgressive surface separating subaerial deltaic and shallow-marine deposits originating during sea-level lowstand from overlying subaqueous deltaic deposits emplaced after the lowstand. Remotely operated vehicle samples of sediment recovered from submerged terrace deposits offshore Santa Catalina Island contain faunal assemblages typical of submerged insular terraces in southern California. The distribution of equivalent extant mollusks and benthic foraminifera indicates deposition in water

depths between 25 and 45 m. Extinct taxa present within the samples provide coarse (Late Pleistocene) age constraints on Santa Catalina's deepest subsided terraces. We identified the transgressive surface corresponding to the Last Glacial Maximum and its paleo-sea-level marker at modern depths between –85 and –95 m surrounding Santa Catalina Island. Terraces surrounding Santa Catalina Island and Pilgrim Banks were correlated to lowstands and interstadials on a glacio-isostatic-adjusted, ice-volume-equivalent sea-level curve in order to evaluate subsidence rates. Santa Catalina Island has been tilting north and subsiding together with its surrounding platform at 0.08–0.27 mm/yr since at least 1.15 Ma (marine oxygen isotope stage [MIS] 34). Pilgrim Banks has been subsiding at 0.3 mm/yr for at least 0.35 m.y. but must have subsided no faster than 0.12 mm/yr between 0.35 and 1.15 Ma. We interpret the subsidence and 1.5° northward tilt of Santa Catalina Island as showing continued, although reduced, activity of the Catalina fault system simultaneous with increasing activity on the southern San Pedro Basin–San Diego Trough fault zone.

## INTRODUCTION

At the coastline of every continent and island, waves and currents distribute sediment and create a detailed stratigraphic record of changes in sea level and vertical tectonic deformation. Mapping coastal vertical motion is necessary for understanding and adapting to changing sea level, and it provides valuable insight into the mechanics of anastomosing faults that transect

the offshore portion of the North American–Pacific plate boundary (Niemi et al., 2008). Marine terraces, wave-planed erosional platforms, and their adjacent constructional sedimentary platforms have been used in the California Continental Borderland to determine Quaternary uplift and subsidence rates and ultimately constrain restraining and releasing linkages along strike-slip fault zones (Muhs et al., 1992; Legg et al., 2007; Chaytor et al., 2008), and to constrain rates of convergence and growth of the Channel Islands and the Western Transverse Ranges (Rockwell et al., 1988; Pinter et al., 2001). Uplifted fossiliferous marine terraces on islands in the California Continental Borderland are typically used to constrain vertical motion following the methodology of Lajoie (1986), who correlated the back-edges (shoreline angles) of radiometrically dated terraces at known elevations to sea-level highstands, assuming linear uplift rates (Muhs, 1982; Muhs et al., 1992). Uplift rates on mainland terraces at the Palos Verdes Peninsula, San Joaquin Hills, and most of the Channel Islands (Fig. 1) have been constrained using dated emergent terraces (Bryant, 1987; Grant et al., 1999). Vertical motion estimates for the California Continental Borderland are based mostly on uplifted terraces, with relatively few quantitative investigations of subsided terraces (Pinter et al., 2003; Niemi et al., 2008; Chaytor et al., 2008).

The use of submerged terraces in constraining vertical motion is well established (e.g., Steinen et al., 1973; Chiocci and Orlando, 1996; Rohling et al., 1998; Chaytor et al., 2008; Passaro et al., 2011). These investigations typically combine bathymetry and high-resolution seismic-reflection images and require

<sup>†</sup>Corresponding author: chriscastillo101@gmail.com.  
<sup>§</sup>sklemp@stanford.edu; jim.ingle@stanford.edu; cpowell@usgs.gov; mark@leggeo.com; robert.francis@csulb.edu.

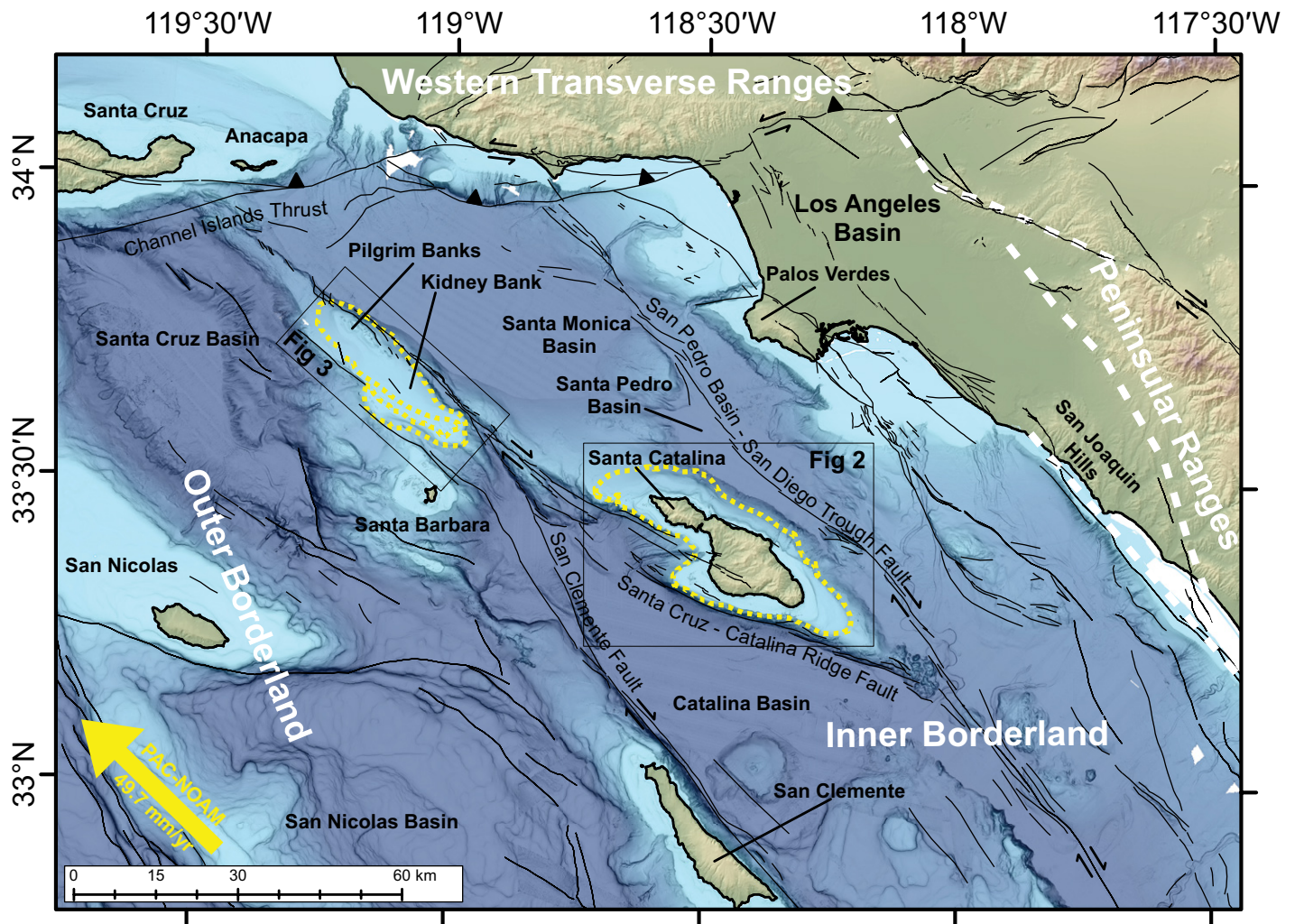


**Figure 1.** Bathymetry and topography of northwestern California Continental Borderland. Faults are in black (adapted from Legg et al., 2015; Francis et al., 2018), major terranes are named in white and bounded by white dashed lines, and distal edges of marine terrace sediments as mapped in this paper around Santa Catalina and Pilgrim/Kidney Banks are outlined with yellow dashed line. PAC-NOAM—Pacific–North American plate.

knowledge of past sea level and recognition of paleo–sea-level markers. However, the paleo–sea-level markers that are most commonly used, the shoreline angle or in situ fossils of known depths, are only accurate to within a few meters at best, and they are difficult to identify in the marine setting (Jardine, 1981). Recent quantitative classification of a globally distributed clinof orm data set provides a criterion for discrimination between subaerial deltas (i.e., beaches) deposited during lowstands and subaqueous deltas deposited during and following transgression, and this allows more precise determination of paleo–sea-level markers using seismic stratigraphy (Patrino et al., 2015). Anacapa and Santa Cruz and Santa Rosa Islands, for example, host emergent terraces from the last interglacial, but bathymetric and seismic data around the islands also reveal submerged terraces that

contain a more extensive record of deformation, back to ca. 0.5 Ma (Pinter et al., 2003). The combination of offshore and onshore data provides a more robust estimate of the rate of convergence and growth along the Channel Islands than uplifted terraces alone.

The vertical motion of the California Continental Borderland has been described as yo-yo tectonics, due to its tortuous vertical motion history (Chaytor et al., 2008). While many of the offshore islands of the California Continental Borderland have experienced uplift during the Quaternary, several submerged and submerging islands and banks stand in contrast, particularly Santa Catalina Island (this paper) and Pilgrim/Kidney Banks (this paper; Chaytor et al., 2008). Whether Santa Catalina Island has experienced Quaternary uplift or subsidence has long been debated (e.g., Lawson, 1894; Legg

et al., 2004b; Muhs et al., 2014). Most neighboring islands clearly bear geomorphic features related to their emergence from the Pacific Ocean, for example, the emergent terraces on San Clemente Island (Muhs and Szabo, 1982). In contrast, Santa Catalina’s rugged landscape contains only sparse and contested evidence of Quaternary uplift (Smith, 1933; Shepard et al., 1939; Loop, 1973; Samaras and Gellura, 1979; Schumann et al., 2012). Miocene–Pliocene marine fossils at the Ben Weston Overlook (Fig. 2, red dot) constrain timing of Santa Catalina’s most recent uplift to no earlier than the Pliocene (Schumann et al., 2012), and certainly following the middle Miocene exhumation of the Catalina Schist from beneath the Peninsular Ranges Batholith (Woodford, 1925; Platt, 1976; Stuart, 1979; Grove et al., 2008). Santa Catalina’s most recent uplift occurred along a

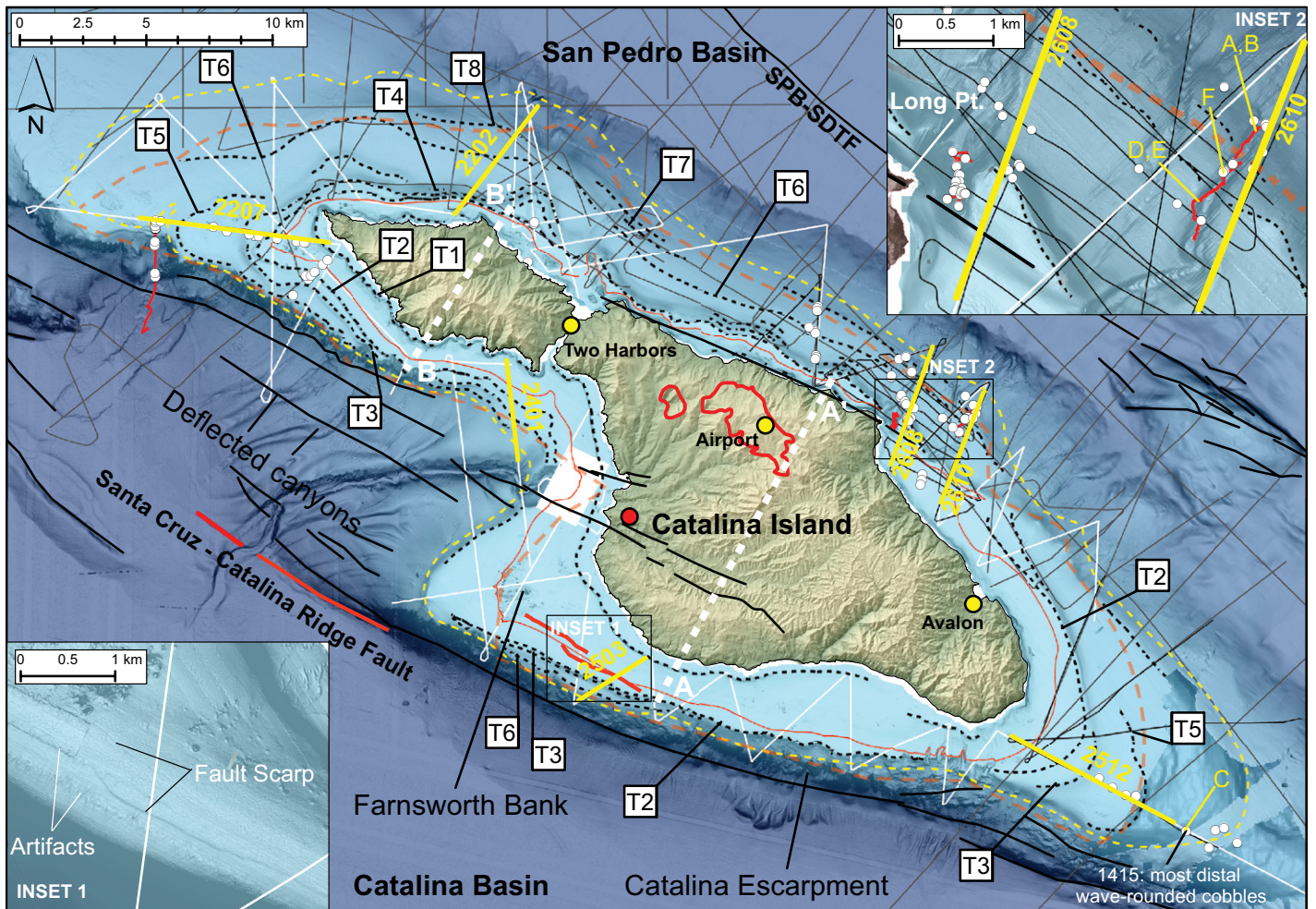


**Figure 2.** Slope-enhanced shaded relief bathymetric and topographic map of Santa Catalina Island, using data sources listed in Table 1. White lines—new Stanford seismic profiles (2014) (white rectangle off west coast is a dense grid), highlighted in yellow if shown in Figure 5. Gray lines—vintage seismic data (see Table 1). Heavy black lines—faults. Orange lines—active faults mapped in this study. Dashed black lines—marine terrace rollovers, numbered T1–T8. Yellow dashed line—distal edge of marine terrace sediments. Dashed orange line—approximate contact between uplifted and truncated Miocene sedimentary rocks (seaward) and igneous/metamorphic basement (shoreward) subcropping beneath terrace sediments. White dashed lines—section A–A' and B–B' profiles for flexural-wavelength estimation. Thin red lines—remotely operated vehicle (ROV) dive tracks. White circles—ROV, core, and grab samples. Red circle—Pliocene sedimentary outcrop (Ben Weston Overlook). Yellow circles—towns (Two Harbors and Avalon). SPB-SDTF—San Pedro Basin–San Diego Trough fault. Inset 1: Slope map of area near Farnsworth Bank. Northwest rupture is close to, but clearly distinct from, a nearby bathymetry track line. Inset 2: Slope-map of ROV dives NA067-1459 and NA075-H1556 (red lines) in submarine canyons north of Avalon. Stanford CHIRP data are shown in black lines. Photo locations for Figure 7 are shown in yellow. Thick red line onshore—extent of garnet-amphibolite unit of Grove et al. (2008).

restraining segment of the Santa Cruz–Catalina Ridge fault zone where it diverges from the San Diego Trough fault and along the Santa Cruz–Catalina Ridge fault (Fig. 1; Legg et al., 2004a, 2007, 2015).

Santa Catalina is unique among southern California's eight major islands in that no clear wave-cut platforms dating from its emergence are currently visible above sea level. To date, no enduring evidence of a Quaternary terrace onshore Santa Catalina Island has been produced, and all previously reported marine terraces have

been revisited and either invalidated or shown to be pre-Quaternary (Schumann et al., 2012). In contrast to islands that have experienced uplift during the late Quaternary Period, Santa Catalina is surrounded by a stair-stepped series of flat to very gently dipping submarine surfaces, extending down to 410 m deeper than modern sea level, that have been interpreted as submerged marine terraces (Emery, 1958; Davis, 2004). Pilgrim Banks has a similar succession of bathymetric terraces that also indicate subsidence (Fig. 3; Chaytor et al., 2008). Here, we

present fossil and seismic stratigraphic evidence that the terraces surrounding Santa Catalina Island and the Pilgrim/Kidney Banks are submerged delta-scale clinoforms deposited dominantly during regression and at the beginning of transgression. We used seismic-reflection profiles to interpret paleo-sea level during formation of these parasequences, and we correlated these features with an ice-volume-equivalent eustatic sea-level curve to establish a likely chronology for the subsidence of Santa Catalina Island. We used the sequence-stratigraphic rela-

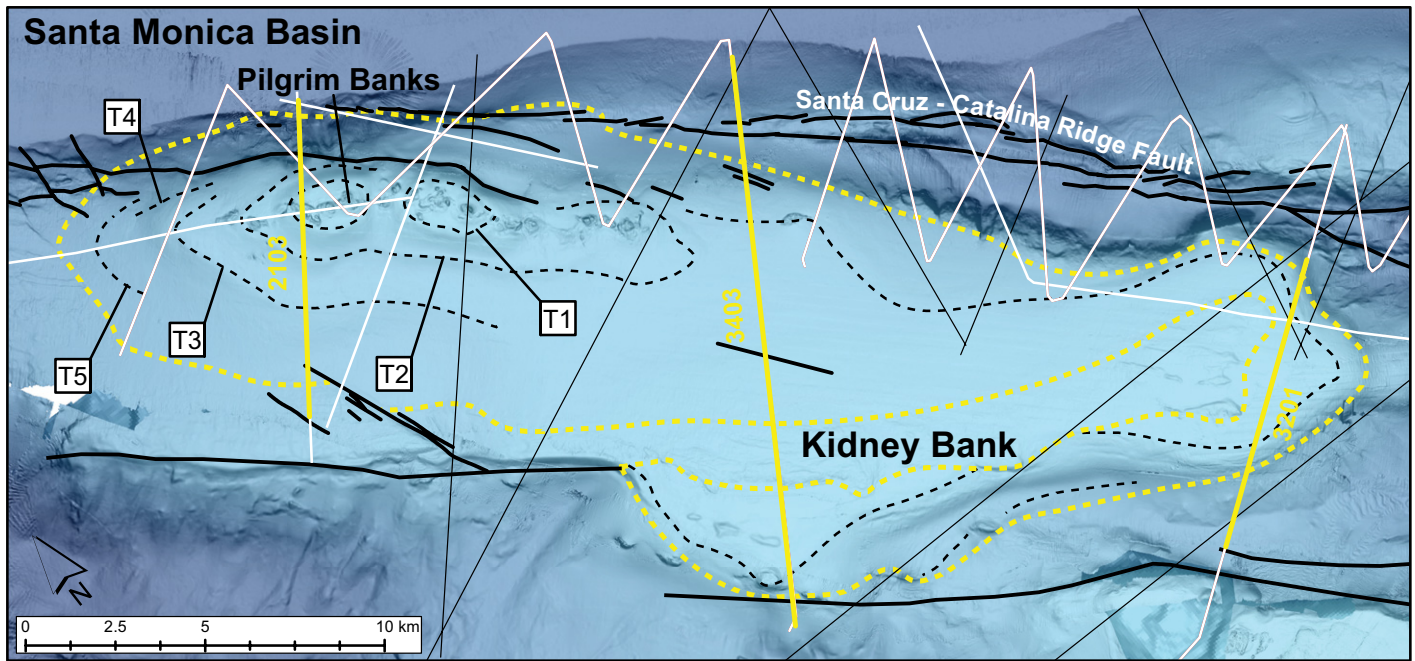


**Figure 3.** Slope-enhanced shaded relief bathymetric map of Pilgrim and Kidney Banks. White lines—new Stanford seismic profiles (2014 and 2016), highlighted in yellow if shown in Figure 6. Fine black lines—vintage seismic data (see Table 1). Heavy black lines—faults. Dashed black lines—marine terrace rollovers. Many areas of map include ship-track-parallel and gridding artifacts.

tionships to show that the terraces surrounding Santa Catalina and the Pilgrim/Kidney Banks require successive sea-level lowstands on a subsiding platform.

## GEOLOGIC SETTING

The Inner Borderland province of the California Continental Borderland is an area of thin continental crust formed during Miocene rifting while the subducted Farallon plate was rapidly exhumed from 40 to 20 km depth (Fig. 1; Legg, 1991; Crouch and Suppe, 1993). The Inner Borderland is bounded on the north by the Western Transverse Ranges at the Channel Islands thrust fault, on the west by the Outer Borderland, and on the east by the Peninsular Ranges (Howell and Vedder, 1981; Shaw and Suppe, 1994). To the south, the Inner Borderland terrane continues as far south as Enseñada Trough, offshore Mexico (Legg, 1991). Subduction of the Farallon plate under southern California ended when the East Pacific Rise contacted North America (Atwater, 1970), causing the initiation of the Inner Borderland Rift, an episode of oblique transtension accompanied by widespread volcanism. During rifting, the Western Transverse Ranges rotated up to 110° clockwise away from the Peninsular Ranges, separating Jurassic basement and Late Cretaceous to Paleogene forearc strata from the western margin of the Peninsular

Ranges Batholith, thereby exposing the Inner Borderland terrane (Luyendyk et al., 1985). The Inner Borderland is currently translating northwest relative to North America along a system of anastomosing strike-slip faults that are part of the greater North American–Pacific plate boundary (Fig. 1; Legg et al., 2015). The northern Inner Borderland is colliding with and being thrust beneath the rapidly uplifting Western Transverse Ranges block along the Channel Islands thrust (Shaw and Suppe, 1994) and is experiencing northeast-directed shortening (Hauksson and Jones, 1988).

Santa Catalina Island is an exposed ridge crest running parallel to the coast of southern California (Figs. 1 and 2), and it is composed primarily of Miocene calc-alkaline volcanic and intrusive rocks, and the Cretaceous Catalina Schist (Grove et al., 2008; Vedder et al., 1979). The northern portion of the island is the type locality for the Catalina Schist, which is inferred from boreholes, outcrops, and seismic profiles to be the basement of the entire Inner Borderland province (Crouch and Suppe, 1993). The southeastern section of the island is composed of Miocene igneous rocks, including the 19 Ma Catalina pluton (Vedder et al., 1979) and several Miocene calc-alkaline dike swarms and flows, in some cases interbedded with marine sediments (Legg et al., 2004b). Small exposures of Cretaceous–Paleogene marine and nonmarine

sediments outcrop on the easternmost portion of the island, and Miocene diatomaceous sediments outcrop on the western portion (Vedder et al., 1979). Miocene sedimentary and volcanoclastic rocks, including the San Onofre Breccia, form less than 5% of the subaerial geology of Santa Catalina, but they also form part of the Santa Cruz–Catalina Ridge, which extends north of the island (Vedder et al., 1986). Pilgrim Banks is a bathymetric high of the larger Kidney Bank platform, and it is composed of Miocene metamorphic and igneous rocks; the western margin of Kidney Bank is the contact between the Inner Borderland and Outer Borderland terranes (Figs. 1 and 2; Junger, 1979; Vedder et al., 1979; Howell et al., 1987). Both the Pilgrim/Kidney Banks and Santa Catalina are mantled by sediments exhibiting terraced morphology that are distinct from the sediments in the Santa Monica, San Pedro, Santa Cruz, and Catalina Basins (Fig. 1; Emery, 1958; Legg et al., 2004b; Chaytor et al., 2008; Francis and Legg, 2010).

## METHODS

### Seismic Data Acquisition, Processing, and Interpretation

We used multiple generations of seismic data, including 1970s U.S. Geological Survey (USGS) boomer and air-gun single-channel

data, 2008–2009 California State University–Long Beach (CSULB) 16 channel sparker data, and 2014 and 2016 Stanford University 36 channel boomer data (Table 1) to interpret sequence stratigraphy, the extent of sedimentation, and bedrock geometry. Stanford seismic data were acquired using a Subsea Systems™ 1.5 kJ triple-plate boomer and a streamer with 3.125 m group interval for channels 1–16 and a 6.25 m group interval for channels 17–36. Navigation data were collected using a Trimble GeoXH™ differential global positioning system and postprocessed before merging with seismic data. Statics were corrected by picking the first arrival on every trace in receiver gathers and smoothing with an 11 trace boxcar filter. Using water sound-velocity profiles collected by E/V *Nautilus* in 2015, data were prestack time migrated (PSTM) in OpenCPS™, yielding an effective vertical resolution of ~0.5 m. Acoustic wave speeds in submerged terrace sediments are within 50 m/s of the acoustic wave speed in water, and all depth conversion was done at 1485 m/s. We applied corrections for tides, streamer, and source depth, and we show depths relative to mean sea level. In addition, we used a digital elevation model (DEM) at 2 m lateral resolution produced by California State University–Monterey Bay (CSUMB)

to generate slope-enhanced shaded-relief raster images (Figs. 2 and 3) that we imported into the IHS Kingdom Suite™ to merge the bathymetry and seismic data.

### Sequence Stratigraphy and Subaerial versus Subaqueous Deltas

Investigating tectonic motion using marine terraces requires accurate determination of paleo-sea level from paleoshoreline indicators (e.g., Pinter et al., 2003; Chaytor et al., 2008; Williams et al., 2018). Uplift rates for emergent marine terraces are calculated by dividing the total vertical motion (the difference between the elevation of the terrace back-edge or “shoreline angle” and sea level at the time of terrace formation) by the age of the terrace (Lajoie, 1986). Successive emergent marine terraces are correlated with episodic sea-level highstands to yield long-term (up to 1 m.y.) Quaternary uplift rates. Similarly, submerged strandlines reflect episodic sea-level lowstands superimposed on a steadily subsiding coastline (Lajoie et al., 1991). However, terrace back-edges in submerged coastal deposits are overlain by coarse landslide-derived sediments, termed boulder wedges, and are difficult to image seismically (Pomar and Tropeano, 2001). Terrace back-

edges only provide a coarse approximation of sea level, and many of the world’s coasts have modern shoreline angles that are up to a few meters above or below the high-tide mark (Pedoja et al., 2011). An alternative paleo-sea-level marker, the subaerial delta clinof orm rollover, is defined in cross section as the point of maximum curvature upslope from the inflection point (e.g., Figs. 4B and 4D). Subaqueous deltaic clinof orm rollovers do not approximate paleo-sea level (Patrino et al., 2015). Clinof orm rollovers are observed at sea level on many of the world’s modern and relict subaerial deltas at the topset of delta-scale clinof orms. The rollover results from decreasing bed shear stress conditions with depth, allowing foresets to be stable at steeper dips in deep water than in the intertidal zone (Pirmez et al., 1998; Keneally, 2016). However, clinof orm rollovers on tectonically stable modern subaqueous deltas occur at depths up to 60 m and thus are not indicative of sea-level position. Delta-scale clinof orms that have been radiometrically dated reveal outer foreset beds much younger than their corresponding lowstand (Kuehl et al., 1986; Alexander et al., 1991) and suggest that the steepest and outermost foreset beds on many shelves are deposited after the lowstand and during transgression or even in highstand conditions.

TABLE 1. SEISMIC AND BATHYMETRIC DATA FOR SANTA CATALINA ISLAND AND SURROUNDING AREAS, SOUTHERN CALIFORNIA, USED IN THIS STUDY

Cruise	Figs.	Platform	Equipment	Year	Source
<b>Bathymetry</b>					
AT15-53	3	<i>Atlantis</i>	SeaBeam 2112	2009	NCEI
AT18-11	2	<i>Atlantis</i>	Kongsberg EM122	2011	NCEI
AT26-06	3	<i>Atlantis</i>	Kongsberg EM122	2013	NCEI
AT26-07	3	<i>Atlantis</i>	Kongsberg EM122	2007	NCEI
BOLT02MV	2	<i>Melville</i>	Kongsberg EM120	2008	NCEI
Chaytor et al. (2008)	3	R/V <i>Velero IV</i>	SimradSM2000	2003	USGS
CNTL04RR	3	<i>Roger Revelle</i>	SeaBeam2100	2003	CSUMB
CSUMB Catalina	2	R/V <i>VenTresca</i>	Reson's SeaBat 7111, SeaBat 7125	2008	CSUMB
CSUMB Farnsworth	2	R/V <i>VenTresca</i>	Reson 8101	2004	CSUMB
CSUMB SBI	3	R/V <i>VenTresca</i>	Reson 8101	2001, 2006	CSUMB
E-1-04-SC	3	<i>Maurice Ewing</i>	Simrad EM1002	2004	NCEI
EX1101	3	<i>Okeanos Explorer</i>	Simrad EM302	2011	NCEI
MV1010	2,3	<i>Melville</i>	Kongsberg EM122	2010	NCEI
MV1010	3	<i>Melville</i>	Kongsberg EM122	2010	NCEI
MV1214	2	<i>Melville</i>	Kongsberg EM122	2012	NCEI
MV1214	3	<i>Melville</i>	Kongsberg EM122	2012	NCEI
<i>Nautilus</i> NA-067	2	<i>Nautilus</i>	Kongsberg EM302	2015	OET
<i>Nautilus</i> NA-074	3	<i>Nautilus</i>	Kongsberg EM302	2016	OET
<i>Nautilus</i> NA-075	3	<i>Nautilus</i>	Kongsberg EM302	2016	OET
<i>Nautilus</i> NA-078	2,3	<i>Nautilus</i>	Kongsberg EM302	2016	OET
NBP0207	3	<i>Nathaniel B. Palmer</i>	Kongsberg EM120	2002	NCEI
OXMZ01MV	3	<i>Melville</i>	SeaBeam2000	1999	NCEI
REVT01RR	2	<i>Roger Revelle</i>	SeaBeam2100	1996	NCEI
WEST15MV	2	<i>Melville</i>	SeaBeam2000	1995	NCEI
<b>Seismic</b>					
CSULB 2008,2009	2	<i>Sea Watch</i> , Yellowfin	2 kJ sparker, 16 channel	2008, 2009	CSULB
Stanford SCITTLES	4,5,6	<i>Jab</i> , Yellowfin	1.5 kJ boomer, 36 channel	2014, 2016	Stanford
USGS Kelez (K-2-73-SC)	2	<i>Kelez</i>	Air gun, uniboom, single channel	1973	NCEI
USGS Lee (L-4-90-SC)	2,3	R/V <i>S.P. Lee</i>	Air gun, multichannel	1990	NCEI
USGS Oil City (O-1-69-SC)	2	<i>M/V Oil City</i>	30–100 kJ sparker, single channel	1969	NCEI
WesternGeco (W-30-81-SC)	2	Unspecified	Air gun, 96 channel	1982	NCEI
WesternGeco (W-5-82-SC)	2	Unspecified	Air gun, 120 channel	1982	NCEI

Note: NCEI—National Center for Environmental Information (<https://www.ncei.noaa.gov/>); USGS—United States Geological Survey (National Archive of Marine Seismic Surveys, <https://walrus.wr.usgs.gov/NAMSS/>); CSUMB—California State University, Monterey Bay (Seafloor Mapping Lab, <http://seafloor.csumb.edu/>); OET—Ocean Exploration Trust; CSULB—California State University, Long Beach ([www.oceanexplorationtrust.org/data-request](http://www.oceanexplorationtrust.org/data-request)).

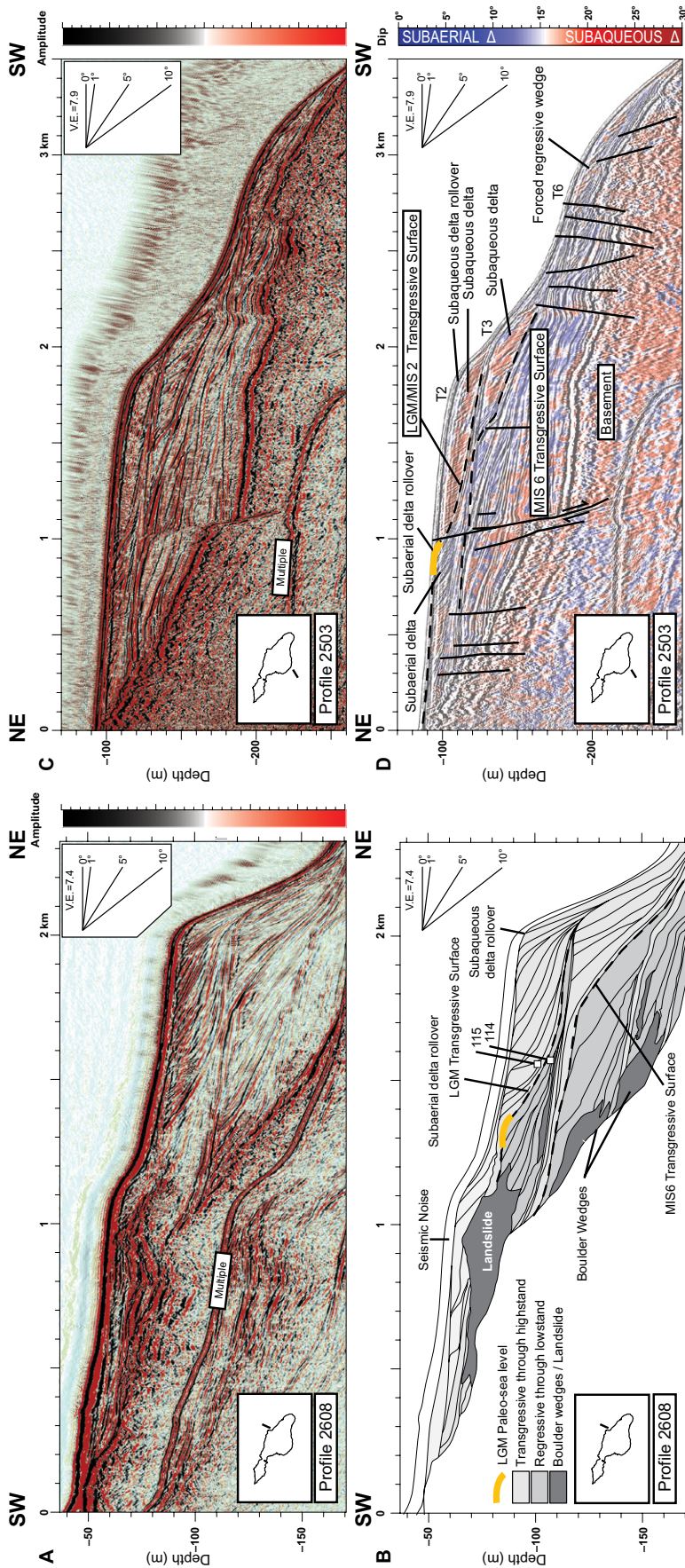


**Figure 4.** (A) Depth-converted, prestack time-migrated Stanford seismic profile 2608 (located in Fig. 2), with color corresponding to seismic amplitude. (B) Interpretation of Stanford seismic profile 2608. Samples NA075-114 and NA075-115 projected updip into their correct stratigraphic positions; size of boxes indicates stratigraphic uncertainty, given range of possible dips estimated from CHIRP cross lines (Fig. 2, inset 2). (C) Depth-converted, prestack time-migrated Stanford seismic profile 2503 (located in Fig. 2), with color corresponding to seismic amplitude. (D) Same data (in black-and-white) overlain by colors representing local dip of high-frequency seismic reflections. Blue corresponds to dips  $\leq 10^\circ$  representative of subaerial deposition. Red corresponds to dips  $\geq 18^\circ$  requiring subaqueous deposition. MIS—marine oxygen isotope stage. V.E.—vertical exaggeration.

Recent quantitative classification of fore-sets in a globally distributed data set (Patruino et al., 2015) constrained the dips of clinoforms, allowing discrimination between low-dip subaerial delta foresets (dip  $< 10^\circ$ ) deposited at lowstands, and steep subaqueous delta foresets deposited during and following transgression (dips up to  $27^\circ$ ). Using these criteria, we distinguished low-dip subaerial deltas, for which the rollover does indicate sea-level position, from outer-shelf deposits with dips too steep for subaerial delta deposition (Fig. 4), which do not indicate sea-level position. The transition between subaerial and subaqueous deltas approximately marks the transgressive surface (Hunt and Tucker, 1992), which we identified on seismic data (Fig. 4, yellow lines) as the contact between low-curvature reflectors with clearly identifiable rollovers and overlying reflections with dips indicative of subaqueous deltaic deposition.

We then calculated subsidence following the methodology of Lajoie (1986), with two notable differences: We used the rollover point of the uppermost subaerial delta deposit instead of shoreline angles, and we tied to sea-level lowstands or low interstadials (except for T1 near Santa Catalina Island, discussed below) adjusted to the lowstand depth of Muhs et al. (2014) (cf. Lajoie et al., 1991). The use of shoreline angles is precluded in this depositional system because any concavity developed at lowstand is destroyed during transgression. Modern shoreline angles observable at any rocky California beach can be found at between 0 and 5 m above sea level and more accurately represent maximum storm surge rather than mean sea level.

### Bottom Sampling and Recovery of Macrofossils and Microfossils

We participated in three remotely operated vehicle (ROV) investigations offshore Santa Catalina Island during 2015 and 2016 as part of E/V *Nautilus* cruises NA-067 and NA-075 (Bell et al., 2016). Dives utilized tandem ROVs, *Hercules* and *Argus*, and were guided via telepresence from Stanford University and Legg Geophysical. During E/V *Nautilus* dive NA-067-H1459, the ROVs were piloted upslope in the submarine canyon north of Avalon between depths of 350 and 230 m (Fig. 2, inset 2), allowing sampling and detailed descriptions of the lithofacies that comprise the sedimentary prism surrounding Santa Catalina Island. Dive NA067-H1560 started at 1100 m, ascended the Catalina Escarpment, and terminated at 130 m depth on terrace surfaces west of the NW tip of the island. Dive NA-075-H1556 targeted the

## Late Quaternary subsidence of Santa Catalina Island from submerged marine terraces

Last Glacial Maximum (LGM) terrace surface between water depths of 125 and 95 m (Fig. 2, inset 2). The LGM transgressive surface is present in outcrop in the two submarine canyons, which have significantly incised the LGM terrace, with the best exposure of LGM strata occurring near Long Point (dive NA075-H1556). We used a combination of multichannel seismic (MCS) and chirp subbottom profiles collected by Stanford University in 2014 and 2015 (Fig. 2, inset 2) to visually identify and navigate to key sedimentary horizons exposed on the walls of the submarine canyon. Poorly consolidated sediment on the canyon walls was collected via suction hose. The number of ROV samples we could collect was limited by storage capacity on the ROV.

Cores and Van Veen samples from Stanford cruises in 2014 and 2015 (white dots on Fig. 2), as well as *Nautilus* ROV grab samples (numbered 001-010, 001-114, 001-115; white dots along red ROV tracks in Fig. 2), were air-dried, sieved, and cleaned for paleontological analysis. We cleaned and scrubbed rocks under tap water and picked identifiable macrofossil remains (Table 2). Samples of soft sediment were washed with water using a 200 mesh Tyler screen (0.074 mm openings) to recover micro-

fossils. Washed residues were then oven-dried. Dried material from each sample was scattered on a gridded metal picking tray and examined under a binocular microscope at 126× and 250× magnification, and representative specimens of benthic and planktonic foraminifera were picked and mounted on microfaunal slides. Specimens were then identified, and counts were made of species abundances in each sample. The relative abundance of each taxon identified was calculated as a percentage of the total number of benthic or planktonic specimens counted in each sample; percentages were not calculated when the total number of specimens in a sample was 50 or less. The number of benthic specimens counted in each sample ranged from 58 to 401 (Table 3), and counts of planktonic specimens ranged from 19 to 312 (Table 4).

Shell material from four bivalve species (samples NA075-114 and NA075-115; Fig. 4B; Table 5) was selected for radiocarbon dating at the Center for Accelerator Mass Spectrometry (CAMS) at the Lawrence Livermore National Laboratory (Davis et al., 1990). Prior to analysis, shells were sonicated in methanol and dried. CALIB 7.10 (Stuiver and Reimer, 1993; Stuiver et al., 2005) was used to correct

the uncalibrated radiocarbon ages using the MARINE13 calibration curve (Reimer et al., 2013). A reservoir correction ( $\Delta R$ ) of  $220 \pm 40$  yr (Ingram and Southon, 1996) was applied to calibrate ages for all samples as listed in Table 5.

## SEISMOSTRATIGRAPHY

Our seismic data show that the sediment package surrounding Santa Catalina, described by Francis et al. (2018), and the sediment package we identified around the Pilgrim/Kidney Banks are composed of multiple stratigraphic sequences (Figs. 5 and 6), some of which have bathymetric expression (Figs. 2 and 3). Each sequence, or terrace, contains three distinct sedimentary units. The most proximal are foresets at relatively low dip ( $<5^\circ$ ) that have truncated tops, and downlapping bottomsets. These are overlain by low-dip foresets with cliniform rollovers observable at their tops (Figs. 4B and 4D). The most distal portion consists of steeply dipping reflectors (up to  $25^\circ$ ), the tops of which are at the same elevation as the tops of the underlying low-dip reflections. The unconformity between low-dip and high-dip cliniforms (white and gray shaded areas in Figs. 5 and 6) is the trans-

TABLE 2. MACROFOSSILS IDENTIFIED IN REMOTELY OPERATED VEHICLE SAMPLES FROM DIVES NA-067-001-010 AND NA-067-020-021

	001	002	003	004	005	006	007	008	009	010	020-021	114	115
Mollusca		x						x	x	x			
Bivalvia											x		
<i>Acila castrensis</i> (Hinds, 1843)													x
<i>Cardiomya</i> cf. <i>C. planetica</i> (Dall, 1908)												x	x
<i>Chlamys hastata</i> (Sowerby, 1842)							x						
<i>Cyclocardia occidentalis</i> (Conrad, 1855)	x					x							
<i>Euvola</i> cf. <i>E. stearnsii</i> (Dall, 1897)			x	x	x		x						
<i>Glans carpenteri</i> (Lamy, 1922)													x
<i>Leporimetis obesa</i> (Deshayes, 1855)							x						
<i>Luciniscia annulata</i> (Carpenter, 1864)													x
<i>Macoma</i> sp.												x	x
<i>Mytilidus</i> sp.				x									
<i>Nuculana</i> cf. <i>N. hamata</i> (Carpenter, 1864)													x
<i>Nutricola</i> cf. <i>N. ovalis</i> (Dall, 1901)												x	x
<i>Nutricola</i> sp.	x											x	
<i>Parvilucina</i> cf. <i>P. approximata</i> (Dall, 1901)												x	
<i>Tellina bodegensis</i> Hinds, 1845							x					x	x
<i>Thyasira flexuosa</i> (Montagu, 1803)													x
Gastropoda										x	x		
<i>Calliostoma</i> sp.												x	
<i>Homalopoma</i> sp.						x							
<i>Mitrella</i> sp.												x	
<i>Pomaulax gibberosa</i> (Dillwyn, 1817)							x						
<i>Puncturella cooperi</i> Carpenter, 1864												x	
<i>Solariella peramabilis</i> Carpenter, 1864													x
<i>Turritella cooperi</i> (Carpenter, 1864)													x
Scaphopoda												x	x
<i>Gadila</i> cf. <i>G. aberrans</i> (Whiteaves, 1887)													
Echinodermata													
Echinoidea													
<i>Strongylocentrotus</i> sp.											x		
Cnidaria													
Anthozoa												x	
<i>Caryophyllia</i> sp.												x	
<i>Desmophyllum dianthus</i> (Esper, 1794)												x	
<i>Lophelia pertusa</i> (Durham, 1947)												x	
<i>Paracythus verrill</i> Verill, 1869												x	

TABLE 3. RELATIVE ABUNDANCE OF BENTHIC FORAMINIFERA IDENTIFIED IN REMOTELY OPERATED VEHICLE SAMPLES FROM DIVES NA-067-002-007, AND NA-067-020-021

	Sample number					
	002	003	004	005	006	007 <sup>†</sup> 020-021
<i>Astronionion incilis</i> (Lankford)	X					X
<i>Astronionion</i> sp.						X
<i>Angulogerina angulosa</i> (Williamson)	X		1			X
<i>Bulimina denudata</i> (Cushman & Parker)	1					X
<i>Angulogerina carinata</i> (Williamson)						X
<i>Angulogerina</i> spp.	X					X
<i>Bolivina acuminata</i> (Natland)						X
<i>Bolivina vaughani</i> (Natland)	X					
<i>Buccella tenerrima</i> (Bandy)					X	
<i>Cancris auricula</i> (Fitchel & Moll)						X
<i>Cassidulina californica</i> (Cushman & Hughes)						1
<i>Cassidulina limbata</i> (Cushman & Hughes)	3		X	6	1	6
<i>Cassidulina</i> spp.		2			2	
<i>Cassidulina subglobosa</i> (Brady)			X	5	1	1
<i>Cassidulina tortuosa</i> (Cushman & Hughes)	20	19	29	25	38	38
<i>Cassidulinoides waltoni</i> (Uchio)				1		X
<i>Cibicides conoidea</i> (Galloway & Wissler)				2	X	X
<i>Cibicides fletcheri</i> (Galloway & Wissler)	32	34	17	17	5	8
<i>Cibicides lobatulus</i> (Walker & Jacob)						
<i>Cibicides mckannai</i> (Galloway & Wissler)		2	X			4
<i>Cibicides</i> spp.	X		X	1		X
<i>Cribrogoesella</i> sp.						X
<i>Dyocibicides biserialis</i> (Cushman & Valentine)	2	3	3	X	2	3
<i>Ehrenbergina compressa</i> (Cushman)						X
<i>Elphidium crispum</i> (d'Orbigny)		3	2	3	13	6
<i>Elphidium</i> spp.		3	X		1	6
<i>Fissurina lucida</i> (Williamson)					1	
<i>Gaudryina arenaria</i> (Galloway & Wissler)	X					
<i>Gavelinopsis companulata</i> (Galloway & Wissler)	6	14	2	19	12	4
<i>Gavelinopsis turbinata</i> (Cushman & Valentine)	9		16	1		
<i>Glabratalia ormitissima</i> (Cushman)	1	3	1		X	
<i>Hanzawaia</i> sp.				1	X	
<i>Haplophragmoides</i> sp.						X
<i>Hoeglundina elegans</i> (d'Orbigny)				5		3
<i>Lagena striata</i> (d'Orbigny)			X			
<i>Nonionella basispinata</i> (Cushman & Moyer)				1		
<i>Patellina corrugata</i> (Williamson)					X	1
<i>Planulina exorna</i> (Phleger & Parker)*	17	2	21	9	2	4
<i>Planulina</i> sp.		4				
<i>Poroepionides cribrerepandus</i> (Asano & Uchio)						2
<i>Pullenia salisburyi</i> (R.E. & K.C. Stewart)						X
<i>Pyrgo</i> sp.						X
<i>Quinqueloculina laevigata</i> (d'Orbigny)						X
<i>Quinqueloculina lamarckiana</i> (d'Orbigny)	2	2	2		10	X
<i>Quinqueloculina</i> spp.		3			6	1
<i>Robulus</i> sp.						X
<i>Rupertia stabilis</i> (Wallach)						2
<i>Sigmomorphina frondiculariformis</i> (Galloway & Wissler)			X		X	
<i>Textularia schencki</i> (Cushman & Valentine)		3	2			X
<i>Triloculina ornata</i> (d'Orbigny)					X	
<i>Triloculina</i> spp.					X	
<i>Trochammina</i> spp.			X			X
<i>Uvigerina juncea</i> (Cushman & Todd)			X			X

Note: See Data Repository Table S1 for sample locations (text footnote 1).

\**P. ariminensis* and *P. ornata* of some authors.

<sup>†</sup>See Figure 7C.

gressive surface. This interpretation is supported by the lithology (Supplementary Table S1<sup>1</sup>), fossil content (Tables 2, 3, and 4), acoustic characteristics, the dip of their foresets (Fig. 4), and the carbon ages (Table 5) of fossils recovered from above and below the transgressive surface. The

elevations of the tops of the subaqueous delta foresets are set by the preexisting bathymetric relief of the underlying abandoned subaerial delta rollover, which provides shelter from bottom currents and hence lower shear stress on the slope than on the tread of the terrace (Mitchell et al., 2012). Although we counted 16 sequences near Santa Catalina Island (Fig. 5, profile 2202, where open circles mark shoreward limit of each sequence), there are only eight terraces with varying bathymetric expression surrounding the island (Figs. 2 and 5, terrace rollovers numbered T1–T8), and even fewer along the Catalina Escarpment.

<sup>1</sup>GSA Data Repository item 2018247, which includes Table S1: Sample locations from Santa Catalina Island; Figure S1: Santa Catalina and San Clemente Island topography and bathymetry; Figure S2: Santa Catalina Island seismic data; and Figure S3: Pilgrim/Kidney Banks seismic data, is available at <http://www.geosociety.org/datarepository/2018> or by request to [editing@geosociety.org](mailto:editing@geosociety.org).

The outer edges of terrace surfaces (Fig. 2) are underlain by steeply dipping foresets that are often acoustically transparent or contain only weak internal reflectivity (Fig. 4). Foresets range in dip from 5° to 27° and often occur in a lozenge-shaped package overlain by a thin cover of muds and bioclastic carbonates (Figs. 7B and 7D). The steeper foresets (>15°) are steeper than any known subaerial delta foresets anywhere on Earth (Patrino et al., 2015), and we interpret them as subaqueous deltas deposited during transgression and even in highstand conditions. Packages of steeply dipping foresets buttress against clinoforms of lower dip that have truncated toplaps above and lapouts below, and that show relatively high reflectivity, positive impedance contrast, and broad rollover (>50 m laterally from shelf to slope) consistent with elevation profiles of modern beaches. These low-dip subaerial deltaic deposits overlie forced regressive clinoforms. Reflections upslope from these low-dip reflections are truncated at or near the seafloor and are sometimes overlain by a thin veneer of sediment (e.g., Fig. 5, profile 2401, sediments above 90 m) deposited during and shortly after transgression. Each horizontally continuous terrace (Fig. 4B) contains, from proximal to distal, regressive deposits, lowstand subaerial deltaic deposits, and subaqueous deltaic sediments deposited during transgression. Thus, each terrace requires base-level change approximately equal to eustatic sea-level fluctuations offshore southern California and therefore must represent one sea-level cycle. This transgressive-regressive succession is repeated in up to 16 parasequences on the northeast side of the island (Fig. 5, profiles 2202, 2610) to four south of the island (Fig. 5, profiles 2503, 2512). Along the southeast margin of the island (Fig. 5, profile 2610), the stratigraphic thickness becomes so small between the ninth and thirteenth sequence boundaries that we could not locate the shelf edge precisely. In contrast to these thin terraces, sequences north of the island (Fig. 5, profile 2202) were thick enough that subaqueous and subaerial deltas could be discriminated down to 470 m water depth. The thickness of sequences varies around Santa Catalina Island, likely due to varying subsidence and sediment-supply histories for different sections of the island.

The basement rocks of Pilgrim Banks are overlain by at least 11 successive parasequences (Fig. 6, profile 2103) similar to those near Santa Catalina (Fig. 5), although only four bathymetric terraces were observed (Fig. 3). Terraces are laterally extensive on the southwest side of Pilgrim Banks (e.g., Fig. 6, profile 2103), but terraces on the northeast side are narrower and have steeper dips (e.g., Fig. 6, profile 3403) than the

## Late Quaternary subsidence of Santa Catalina Island from submerged marine terraces

TABLE 4. RELATIVE ABUNDANCE OF PLANKTONIC FORAMINIFERA IDENTIFIED IN REMOTELY OPERATED VEHICLE SAMPLES FROM DIVES NA067-002–007 AND NA067-020–021

Planktonic species <sup>†</sup>	Sample number							Last appearance in fossil record
	002	003	004	005	006	007	020–021	
<i>Globigerina bulloides</i> (d'Orbigny)	42	34	42	X*	X*	44	27	
<i>Globigerina falconensis</i> (Blow)							X	
<i>Globigerina quinqueloba</i> (Natlund)	2	4				10	4	
<i>Globininerella aequilateralis</i> (Brady)							X	
<i>Globigerinoides ruber</i> (d'Orbigny)	1		1	X*		2	4	
<i>Globigerinoides</i> sp.							X	
<i>Globigerinita uvula</i> (Ehrenberg)	3		X			X	1	
<i>Globorotalia crassaformis</i> (Galloway & Wissler)	X		1				X	0.2 Ma
<i>Globorotalia hirsuta</i> (d'Orbigny)							X	
<i>Globorotalia inflata</i> (d'Orbigny)							X	
<i>Globorotalia tosaensis</i> (Takayanagi & Saito)							X	
<i>Globorotalia truncatulinoides</i> (d'Orbigny)							1	0.61 Ma
<i>Neogloboquadrina dutertrei</i> (d'Orbigny)				X*		X	16	
<i>Neogloboquadrina incompta</i> (Cifelli) <sup>§</sup>	11	24	14	X*	X*	32	38	
<i>Neogloboquadrina inglei</i> (Kucera & Kennett)							2	0.7 Ma
<i>Neogloboquadrina pachyderma</i> (Ehrenberg) <sup>#</sup>	38	37	40	X*	X*	10		
<i>Neogloboquadrina</i> sp.							X	
<i>Orbulina universa</i> (d'Orbigny)	1						4	

<sup>†</sup>Percent of total number of specimens counted in each sample; X = <1%; X\* = less than 50 specimens counted in sample.

<sup>§</sup>Dextral coiling forms formerly assigned to *N. pachyderma* (see Darling et al., 2006).

<sup>#</sup>Sinistral coiling specimens.

terraces on the southwest side of the banks. The Santa Cruz–Catalina Ridge fault dissects the terraces on the northeast side of the Pilgrim Banks, making sequence interpretation problematic in our existing data (Fig. 6, profile 3403). On Kidney Banks, “terraces of unknown age” (Fig. 6, profiles 3403 and 3201) are likely equivalent to marine oxygen isotope stage (MIS) 10 to MIS 30, based on their depths.

The most laterally extensive bathymetric terraces surrounding Pilgrim Banks (T4: Figs. 3 and 6) and Santa Catalina Island (T6: Figs. 2 and 5) are underlain by stratigraphically similar sequences that share similar architecture and elevation distribution. We correlated the terraces between Santa Catalina Island and Pilgrim Banks based on the similarity of distinct forced regressive strata identified from their prograding and downstepping stacking patterns (Figs. 5 and 6, MIS 14/16 forced regressive wedge; Hunt and Tucker, 1992), which are overlain by five clear sequences around Santa Catalina Island and Pilgrim Banks. This suggests a minimum age (see discussion, below) of ca. 530 ka (MIS 14) for

T6 at Santa Catalina and T4 at Pilgrim Banks. At Pilgrim Banks, the distinct forced regressive wedge is also overlain by five sequences, although the uppermost terrace at Pilgrim Banks is thin compared to the uppermost sequences near Santa Catalina Island, presumably owing to decreasing availability of detrital material on the subsiding banks, which are separated by deep water from any other terrestrial source. It is known that the upper surface at Pilgrim Bank (Fig. 3, T1) last experienced deposition during the LGM (Chaytor et al., 2008).

### Lithology

The terrace sediments around Santa Catalina Island are composed of conglomerates, sandstones, and siltstones interbedded with biouridites, and minor landslide deposits (Fig. 7; Table 1). We found no evidence that sediments in the terrace package surrounding Santa Catalina Island were sourced from anywhere but the island. We recovered rounded cobbles from the seafloor around the island in Van Veen samples

from as deep as 218 m and 8.6 km offshore along profile 2512, Stanford sample 1415 (Figs. 2 and 7C). Similar cobbles have been recovered by other researchers from dredge hauls several kilometers from the modern shoreline (Ritter, 1901). We also identified rounded cobbles during ROV dives in conglomerate beds within the terrace sequence (Figs. 7B and 7D). Their widespread distribution (some far removed from rivers) suggests a nonfluvial origin, likely in the intertidal zone. Although the local Los Angeles Basin Gabrieleno-Tongva Native Americans transported significant numbers of wave-rounded stones around the island (Glassow, 1980), they cannot account for rounded cobbles widely distributed far offshore within Santa Catalina's deepest, oldest terraces.

Sample NA067-001 (Fig. 5, profile 2610) is a sandy limestone composed of mostly shell fragments and quartz grains with <2% lithic grains. Samples NA067-002 (Fig. 5, profile 2610) through NA067-008 and NA067-010 are bioclastic marls typical of insular submerged terrace and bank tops in the California Continental

TABLE 5. ACCELERATOR MASS SPECTROMETRY (AMS) <sup>14</sup>C RADIOCARBON AGES OF REMOTELY OPERATED VEHICLE SAMPLES FROM SUBMARINE CANYON NORTH OF SANTA CATALINA ISLAND

Sample	Ocean Exploration Trust			Species	Data from LLNL			Calibrated ages			
	Longitude (°W)	Latitude (°N)	Depth (m)		CAMS no.	<sup>14</sup> C age (yr)	±	1σ age (yr B.P.)	2σ age (yr B.P.)	1σ age (yr B.P.)	2σ age (yr B.P.)
NA075-114C-01	118.3613	33.4051	115.5	<i>Tellina bodegensis</i> (Hinds, 1845)	176333	41,650	740	<b>45,244</b>	<b>43,913</b>	<b>45,809</b>	<b>43,264</b>
NA075-114C-02	118.3613	33.4051	115.5	<i>Nutricola</i> sp.	176347	35,670	360	<b>40,069</b>	<b>39,200</b>	<b>40,466</b>	<b>38,805</b>
NA075-114C-03	118.3613	33.4051	115.5	<i>Nutricola</i> sp.	176359	45,500	1200	<b>49,455</b>	<b>47,099</b>	<b>50,068</b>	<b>46,171</b>
NA075-115C-01	118.3612	33.4054	104.5	<i>Nuculana</i> cf. <i>N. hamata</i> (Carpenter)	176334	40,240	630	<b>43,924</b>	<b>42,881</b>	<b>44,520</b>	<b>42,501</b>
NA075-115C-02	118.3612	33.4054	104.5	<i>Tellina bodegensis</i> (Hinds, 1845)	176348	14,910	60	17,592	17,347	17,683	17,215
NA075-115C-03	118.3612	33.4054	104.5	<i>Tellina bodegensis</i> (Hinds, 1845)	176360	11,670	40	13,071	12,886	13,156	12,816

Note: Samples older than the Last Glacial Maximum (LGM) are in bold. LLNL—Lawrence Livermore National Laboratory.

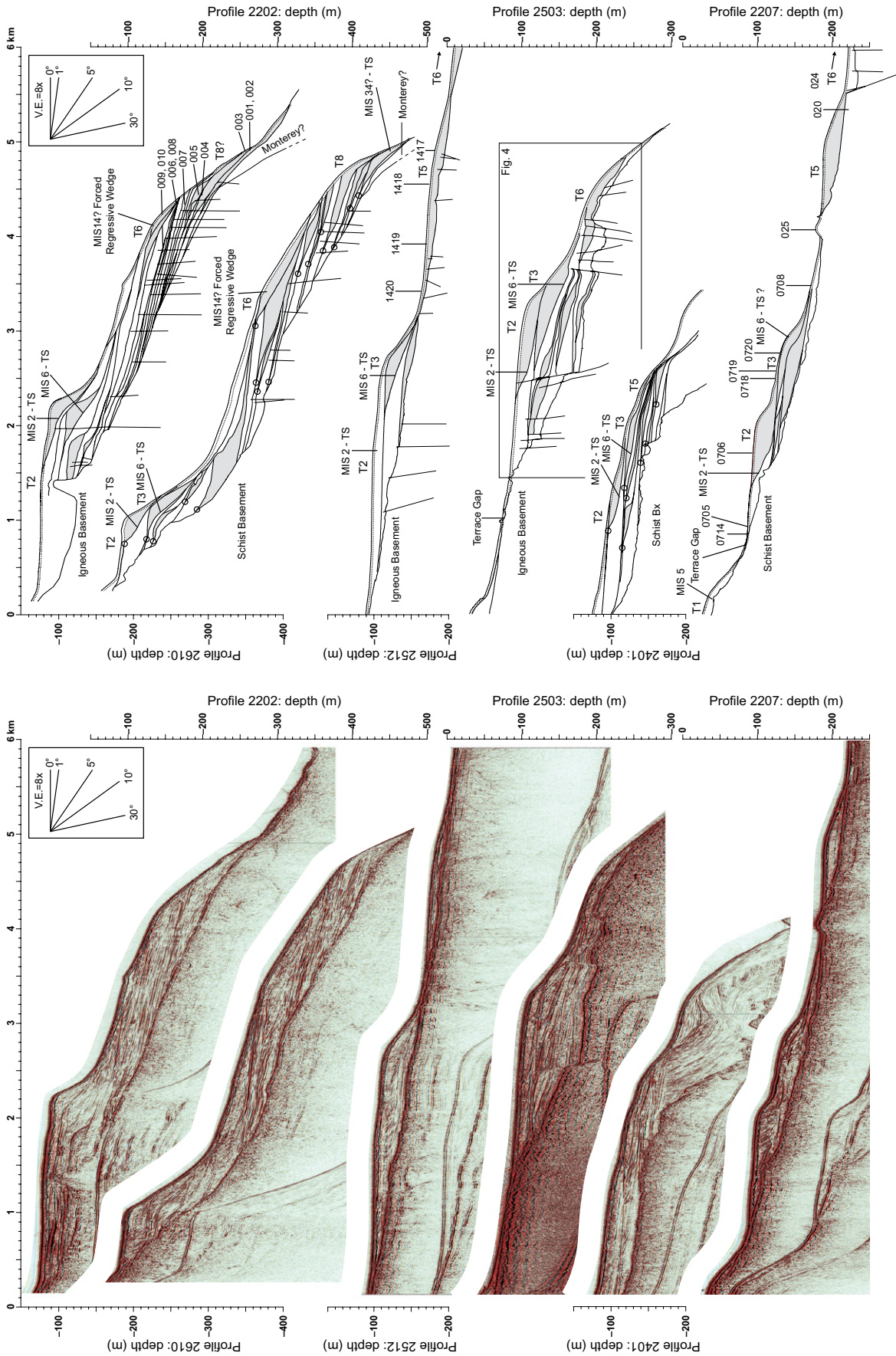


**Figure 5.** Depth-converted, prestack time-migrated Stanford seismic profiles (left) and their interpretations (right) around Santa Catalina (locations in Fig. 2). Right panel: labeled bathymetric terraces (T1–T8) match numbering of Figure 2. Sequence boundaries and transgressive surfaces (TS) are labeled by their interpreted marine isotope stage (MIS). Shoreward limits of deltaic sequences are indicated by open circles on profiles 2202 (16 sequences) and 2401 (7 sequences). Sample numbers from remotely operated vehicle (ROV) dives (three-digit numbers, profiles 2610 and 2207) and Stanford grab samples (four-digit codes, profiles 2512 and 2207) are keyed to approximate sample locations (shown as subsurface where the ROV dive sampled canyon walls adjacent to the seismic profile outside the canyon). Subaqueous deltas are shaded gray. Vertical exaggeration (V.E.) = 7.9x.

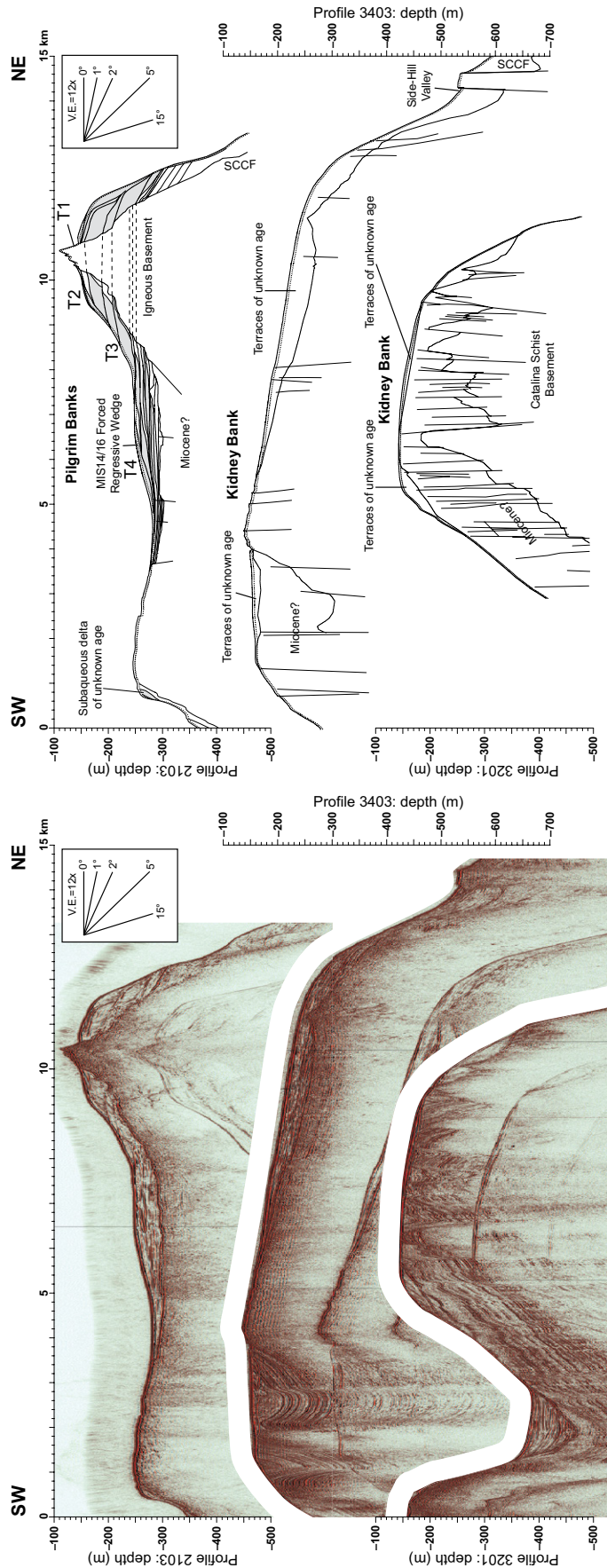


Figure 6. Depth-converted, prestack time-migrated Stanford seismic profiles (left) and their interpretations (right) around Pilgrim/Kidney Banks (locations in Fig. 3). Annotation is as in Figure 5, but vertical exaggeration (V.E.) = 12.1x. SCCF—Santa Cruz–Catalina Ridge fault. MIS—marine isotope stage. Terraces are numbered shallow to deep and do not correspond to Santa Catalina terrace numbers in Figure 5.

Borderland (Douglas et al., 1980) and are composed largely of bryozoan and molluscan shell fragments, tests of benthic and planktonic foraminifera, ostracode valves, echinoid spines, and sponge spicules (Fig. 7E). Preservation of benthic and planktonic foraminifera ranges from poor to moderately well preserved, with many samples showing evidence of dissolution and recrystallization. Sample NA067-009 is a fine-grained sandstone with mollusk fragments and minor bioclastic fragments. Samples NA067-020 and NA067-021, collected near an exposure of igneous rock that protrudes through the marine terrace package at ~230 m depth north of Santa Catalina Island near the Santa Cruz–Catalina Ridge fault (Fig. 5, profile 2207), are foraminiferal-rich silts with abundant *Lophelia pertusa* corals within the sediment. Other units observed during the 2015 ROV dives included sand-rich beds containing a single-species death assemblage of the bivalve mollusk *Euvola stearnsii* (Fig. 7F), and 1–2-m-thick lithic sandstones.

**Macrofossils**

Mollusks recovered from samples NA067-002–NA067-007 (Fig. 5, profile 2610; Fig. 7E; Table 2) provide chronologic and paleodepth information (Fig. 8). All mollusks lived in the epipelagic zone at a maximum depth of ~200 m. The extinct bivalve *Cyclocardia occidentalis*, recovered from NA067-006, is a shallow infaunal suspension-feeder found from the Pliocene to Middle Pleistocene in southern California (Moore, 1992). Today, the genus *Cyclocardia* off California occurs at inner- to outer-shelf depths (15–200 m; Coan et al., 2000). *Chlamys hastata*, recovered from sample NA067-004, has a modern geographic range from the Gulf of Alaska south to San Diego, California, in water depths from the intertidal zone to 150 m (Coan et al., 2000) and occurs in formations as old as late Miocene, as interpreted from formations listed in Moore (1984).

Sample NA067-007 (Fig. 7E) contains the gastropod *Pomaulax gibberosa*, found at water depths between the intertidal zone and greater than 17 m (Keen, 1971), and the bivalve *Leporimetis obesa*, which occurs from the deep intertidal zone to ~50 m (Coan et al., 2000). *Astraea gibberosa* limits the depth of deposition for this sample to probably less than 20 m. *Euvola stearnsii*, identified in samples NA067-003, NA067-005, and NA067-007, is extinct and limits the youngest age of these terraces to middle Pleistocene, based on formations in which it occurs as listed in Moore (1984).

Sample NA075-114 was recovered from low-dip clinofolds that immediately underlie a

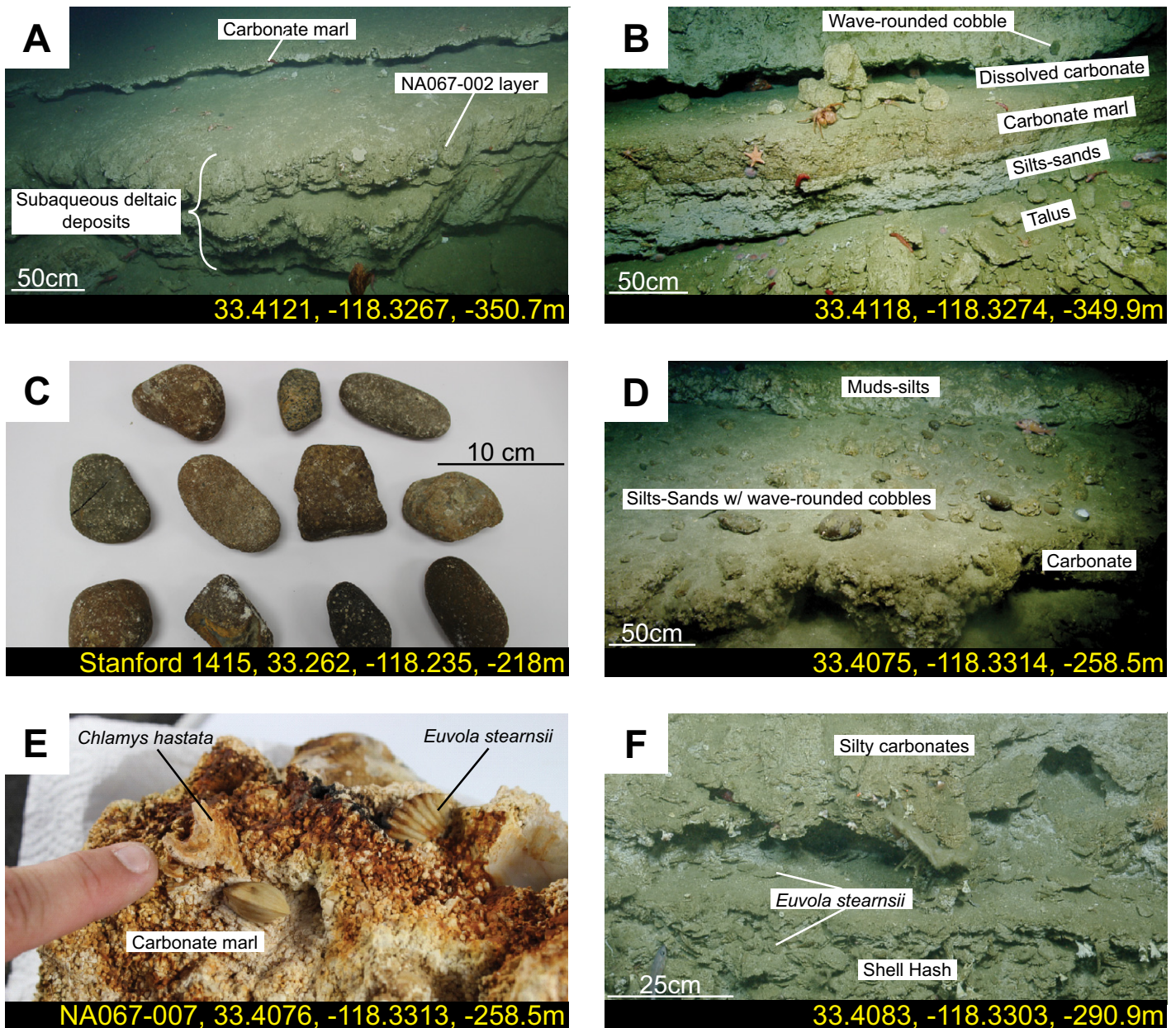


**Figure 7.** (A) Remotely operated vehicle (ROV) photograph of interbedded carbonates and detrital clastic rocks deposited near sea level, now at 351 m depth (Fig. 2, inset 2; Fig. 5). (B) ROV photograph of interbedded carbonates and rounded cobble-bearing sediments deposited near sea level, now at 350 m (Fig. 2, inset 2; Fig. 5). (C) Rounded cobbles from Stanford Sample 1415, from 8 km offshore and 218 m depth. (D) ROV photograph of rounded cobbles weathered out of terrace sediments (Fig. 2, inset 2; Fig. 5), now at 259 m depth. (E) Sample NA067-007, highly cemented carbonate marl with the extinct bivalve *Euvola stearnsii*, collected close to photograph D. (F) ROV photograph of death assemblage containing extinct *Euvola stearnsii* bivalves (Fig. 2, inset 2; Fig. 5).

transgressive surface (Fig. 4B; Tables 2 and 5). We exploited submarine canyons that incise into the 90-m marine terrace surrounding the island (Fig. 2, T2), navigating the *Hercules* ROV from shore using MCS and CHIRP data (Fig. 2, inset 2) and sampling sediments using a suction sampler. We were able to recover only a small amount of material from these clinofolds. Species from this sample restrict its depth of

deposition likely to between 50 m, based on the shallowest occurring gastropod *Solariella peramabilis* (50–350 m; McLean, 1996), and 100 m (deepest occurrence of the bivalve *Glans carpenteri* [0–100 m]; Coan et al., 2000). All taxa in NA075-114 still occur at the latitude of Santa Catalina Island, and none is age diagnostic. However, calibrated radiocarbon ages (Table 5) on three bivalves from this sample

immediately below a transgressive surface (Fig. 4B) span 50–39 ka (MIS 3). Equivalent ages for two bivalves from sample NA075-115 taken stratigraphically just above the same transgressive surface span 18–13 ka (MIS 2), and ages for a third bivalve span 45–43 ka, likely reworked from a deeper horizon. Because foresets are deposited via avalanching of sediments that accumulate at the shelf edge (Pomar and Tropeano,

## Late Quaternary subsidence of Santa Catalina Island from submerged marine terraces

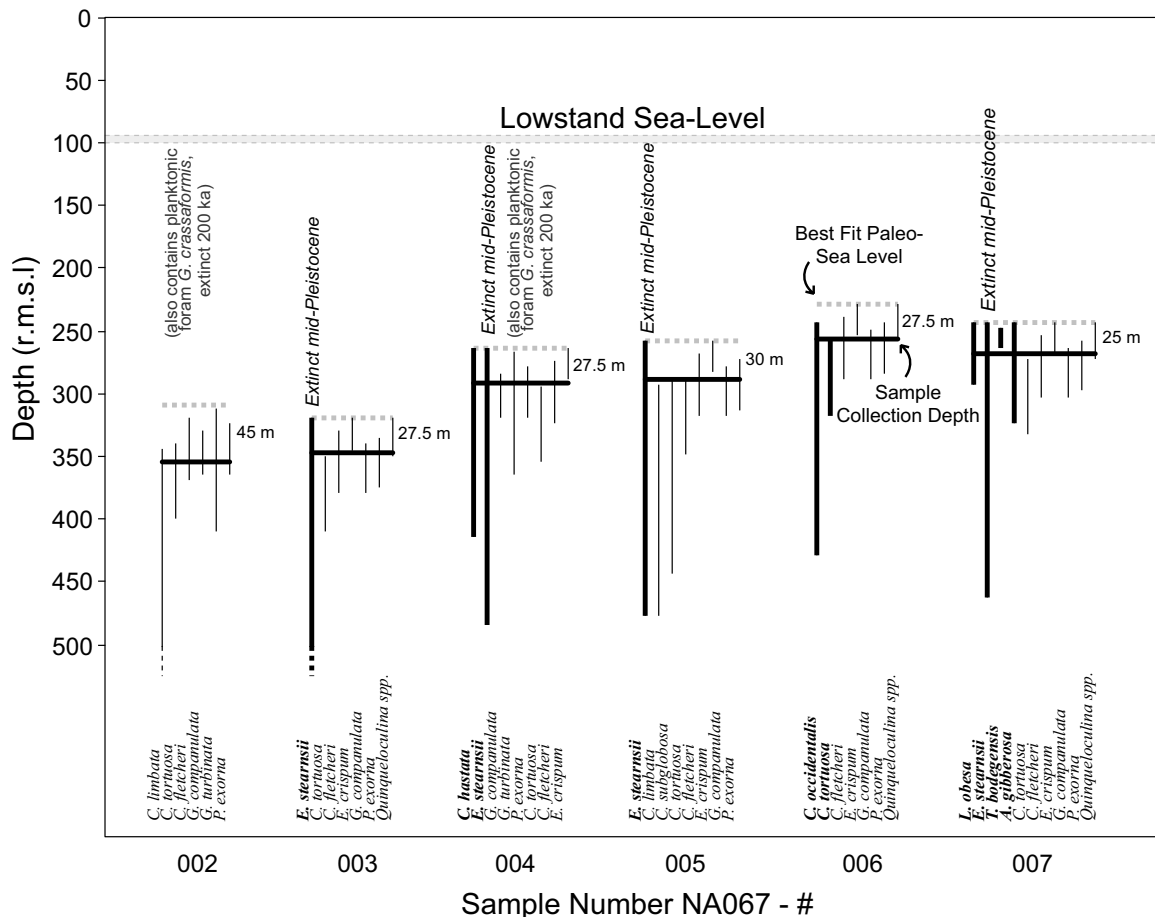


**Figure 8.** Subsidence data from fossils, with macrofossils in red and benthic foraminifera in black. Thick black line—modern depth at which the sample was collected. Thick dashed gray line—best-fit paleo—sea level for the assemblage of fossils recovered in each sample based on depth ranges of foraminifera (thin vertical lines) or mollusks (thick vertical lines) of species living today. Horizontal light-gray bar at 90–100 m represents typical lowstand sea level in the late Quaternary; r.m.s.l.—relative mean sea level.

2001), samples will necessarily contain a low proportion of articulate bivalves, and they were likely subjected to some reworking at least once prior to deposition. Though additional sampling and dating are needed, samples NA075-114 and NA075-115 appear to bracket the LGM, implying they are separated by the post-LGM transgressive surface.

#### Microfossils

##### *Paleoenvironmental Significance of Benthic Foraminifera*

All of the species of benthic foraminifera identified are still living within the continental borderland off southern California and northern Baja California, Mexico, as documented in a number of reports (e.g., Walton, 1955; Zalesny, 1959; McGlasson, 1959; Uchio, 1960; Douglas, 1981). In particular, several studies have focused on the distribution of modern shelf

(neritic) and littoral faunas in this region (e.g., Resig, 1960; Cooper, 1961; Bandy, 1963; Bandy et al., 1964; Lankford and Phleger, 1973; Argow, 1999; McGann, 2002, 2009). Thus, the modern distributions of the benthic species identified in this study are reasonably well established, and we used these data to interpret the environment and water depths at time of deposition of the samples analyzed in this study.

Douglas (1981) made a comprehensive study of benthic foraminifera in the California Continental Borderland and recognized eight recurrent benthic faunal assemblages characteristic of (1) offshore bank and terrace deposits with a mean upper water depth of 50 m, and (2) offshore ridge and deep bank assemblages with a mean upper water depth of 150 m. Five of the benthic species characterizing Douglas' (1981) offshore bank and terrace assemblage, including *Cassidulina limbata*, *Cassidulina subglobosa*, *Cassidulina tortuosa*, *Cibicides fletcheri*,

and *Gavelinopsis (Rotorbinella) companulata*, together comprise 48%–68% of the benthic assemblages identified in samples NA067-002 through NA067-020 (Fig. 5, profiles 2610, 2207). Therefore, we interpret these sample assemblages as representing similar depositional settings and water depths to those of the modern offshore bank and terrace assemblage of Douglas (1981).

*Cassidulina tortuosa* is the most abundant benthic species in the samples we analyzed, with relative abundances of 20%–46% in these assemblages. The depth range of maximum relative abundances of *C. tortuosa* in the modern California Continental Borderland is 34–91 m, with a mean depth of 59 m (Walton, 1955; Zalesny, 1959; Uchio, 1960). The nine species comprising 5% or more of the fossil benthic assemblages in our samples have their maximum living abundances at water depths from littoral through neritic depths. Similar patterns of liv-

ing benthic species were recognized by McGann (2002) through Q-mode cluster analysis of census data recorded by Zalesny (1959) in Santa Monica Bay, California, where an outer-shelf assemblage marked by *C. tortuosa* and *C. limbata* ranges from 59 to 137 m water depth.

The living depth ranges and abundance patterns of the nine most abundant benthic taxa in samples NA067-002 through NA067-007 (Table 3; Fig. 8) suggest that the sediments containing these assemblages were deposited at water depths of 25–45 m. The shallowest-dwelling taxa in these assemblages include *Quinqueloculina* spp., *Elphidium* spp., and *E. crispum*, all of which have their maximum living abundances at littoral to neritic water depths. However, both broken and whole specimens of these species commonly show evidence of abrasion, indicating some degree of transport. Other taxa, including *Gavelinopsis companulata*, are common to abundant at midshelf depths, while *Cassidulina limbata* and *C. subglobosa* range to the shelf edge and upper slope in the modern California Continental Borderland. Benthic foraminifera in sample NA067-020 included higher abundances of *C. limbata*, indicating this sediment may have been deposited at a water depth of ~100 m.

Previous studies of onshore Pleistocene marine deposits in southern California found foraminiferal assemblages similar in character to those analyzed in this study and reflect deposition at littoral to neritic water depths. For example, Douglas (1981) recognized that his living offshore bank and terrace assemblage is similar to the foraminiferal fauna described by Galloway and Wissler (1927) from the middle Pleistocene Lomita Marl, exposed along the flank of the Palos Verdes Hills, which represents an uplifted former island in the evolving California Continental Borderland. Similar benthic assemblages have also been reported from the early to middle Pleistocene Santa Barbara Formation (Patterson et al., 1990) and Pleistocene terrace deposits exposed on San Clemente Island (Lipps, 1967) and Santa Barbara Island (Lipps et al., 1968) in the California Continental Borderland region.

To summarize, the fossil benthic foraminiferal assemblages identified in samples NA076-002 through NA067-007 and NA067-20 are characteristic of both modern and Pleistocene neritic/shelf marine terrace assemblages reported from multiple sites in the California Continental Borderland. Moreover, the species compositions of these assemblages are quite distinct from those at the water depths of 230–354 m from which they were sampled. Benthic foraminiferal assemblages typically found living at upper-slope water depths (>130 m) in the California Continental Borderland are

dominated by *Bolivina* spp., *Epistominella sandiegoensis*, *Globobulimina pacifica*, *Suggrunda eckisi*, and *Uvigerina* spp. (Douglas, 1981), a composition that stands in sharp contrast to those found at neritic water depths. In addition, if the assemblages observed in our samples had experienced downslope transport to upper-slope water depths after initial deposition, they would contain significant admixtures of species typical of these latter depths, or even be completely dominated by upper-slope taxa. Thus, we view the assemblages in our samples as in situ evidence of water depth at time of deposition. In addition, the consistency of paleo-sea levels predicted by each of six to ten species within each sample (Fig. 8), and the consistency between samples of modern sampling depth and predicted paleo-sea level (also Fig. 8) strongly suggest that our paleontologically determined paleo-sea levels from individual samples are accurate within 10 m.

#### **Paleotemperature and Age Significance of Planktonic Foraminifera**

The abundance of planktonic foraminifera in samples NA067-002 through NA067-007 ranged from common to sparse, and their preservation was generally poor. A more diverse and well-preserved assemblage was present in sample NA067-020. Sixteen species were identified in this sample (Table 4), of which all but three are known to be living in the modern California Continental Borderland.

Significant changes in the composition of Holocene–Pleistocene planktonic foraminifera have occurred in the California Continental Borderland over the Pleistocene as a result of global and regional paleoclimatic and paleoceanographic events (e.g., Kennett and Venz, 1992; Lyle et al., 2000; Hendy, 2010). Aspects of these changes are clearly reflected by differences in the planktonic assemblages in samples NA067-002 through NA067-020. For example, relatively high abundances of sinistral coiling forms of *Neogloboquadrina pachyderma* in samples NA067-002–NA067-004 mark times of cooler sea-surface temperatures. In contrast, the absence of sinistral coiling specimens of *N. pachyderma* in sample NA067-020 and the presence of relatively high abundances of *Neogloboquadrina incompta* and warmer-water species, including *Neogloboquadrina dutertrei* and *Globigerinoides ruber*, indicate warmer surface temperatures.

Three species of planktonic foraminifera provide limited evidence of age for samples NA067-002, NA067-004, and NA067-020. Net-tow and sediment-trap studies of planktonic foraminifera in the marginal northeastern Pacific Ocean indicate that *Globorotalia crassaformis*

is no longer present within living assemblages in this region (e.g., Sautter and Thunell, 1991), although it is living elsewhere in the global oceans. Significantly, *G. crassaformis* is commonly found in Pliocene through Pleistocene assemblages in onshore and offshore deposits in the southern California region and elsewhere along the Pacific Coast of North America. Accumulating evidence suggests that *G. crassaformis* became regionally extinct at ca. 200 ka. If this pattern is confirmed, the presence of this taxon in samples NA067-002 and NA067-004 indicates that these samples are no younger than 0.20 Ma. The planktonic assemblage in sample NA067-020 includes two extinct species, *Globorotalia tosaensis* and *Neogloboquadrina inglei*. The last appearance of *G. tosaensis* is 0.61 Ma (Wade et al., 2011), and the last appearance of *N. inglei* is ca. 0.70 Ma (Kucera and Kennett, 2000). Based upon the presence of these two stratigraphically restricted species, these sediments are no younger than 0.70–0.60 Ma.

#### **DISCUSSION**

We have presented the evidence that regressive to transgressive sequences are preserved around Santa Catalina at depths greater than 400 m (Fig. 5), that intertidal facies in the form of wave-rounded cobbles are present to at least 350 m water depth (Fig. 7), and that benthic foraminiferal and molluscum assemblages, including taxa that became extinct by the Middle Pleistocene, collectively indicative of depositional water depths <50 m are now present below 300 m (Fig. 8). These modern water depths of Middle Pleistocene littoral facies greatly exceed the deepest Pleistocene paleo-sea levels of ~100 m and require correspondingly large tectonic subsidence. We identified the subsided LGM transgressive surface, with its paleo-sea-level marker, between 85 and 100 m (Figs. 4B and 4D, highlighted yellow), consistent with LGM paleo-sea-level estimates in the California Continental Borderland of ~95 m (Muhs et al., 2014). We next review our model for terrace development, discuss possible caveats, and then consider the timing, causes, and rates of vertical motion of Santa Catalina Island and the Pilgrim/Kidney Banks.

#### **Terrace Development Model**

Whereas uplifted terraces are formed mostly during highstands, submerged terraces are relatively complex systems that are formed during all phases of eustatic sea-level change, i.e., transgressive and regressive cycles (Miall, 2010). On a subsiding margin, basement is first exposed to erosion by waves during highstand

events. In highstand conditions, the coarsest-grain deposits, boulder wedges, are developed from the eroding bedrock, while finer material is carried downslope (Pomar and Tropeano, 2001). Subaerial deltas with gravel- to sand-rich beaches, both fluvially and coastally supplied, form in areas of relatively high sediment supply or where waves and coastal configurations are favorable to stable beaches. In the absence of fluvial supply, sediment sourced by wave-induced erosion of exposed basement or landslide deposits is mobilized directly by wave energy and is transported downslope. Significant landslides observed during the M 5.3 earthquake near Santa Cruz Island on 5 April 2018 suggest that seismically triggered landslides supply significant amounts of sediment to the shelf. The finest-grained suspended sediments are entrained in currents and redistributed in subaqueous deltas, while coarser material is transported as bed load. Landslide deposits are common in the most proximal portions of each terrace (Figs. 4A and 4B) and are seismically distinct from finer-grained subaerial and subaqueous deltaic deposits. Following the highstand, wave base drops as regression begins, and poorly consolidated sediments deposited during the highstand are eroded and redeposited downslope (Miall, 2010). This process continues throughout the regression and accounts for the area of thin sediments between the modern shallow subaqueous delta deposits and the deeper terrace sediments comprising the outer shelf (Fig. 5, profile 2503, 70–85 m depth, and profile 2207, 75–85 m depth). These falling-stage systems tract strata are the proximal sediments in each terrace (non-shaded portions of terrace packages in Figs. 5 and 6), and they contain variations in dip that may be signals of fourth-order and suborbital-scale sea-level fluctuations.

Lowstand terrace deposits are the culmination of millennia of cannibalistic downslope transport of sediment. The final signal of a lowstand is the paleoshoreline (Fig. 5, profile 2202, black circles) and its low-dip reflectors with clear roll-overs at the top (Fig. 4). Sample NA075-114, collected immediately below our mapped LGM transgressive surface (Fig. 4B), is composed of unconsolidated sand containing several rounded cobbles and abundant shell fragments, and it contains bivalves with radiocarbon ages all older than the LGM (corresponding to MIS 3; Table 5) and fossil assemblages indicative of water depths of 25–100 m. During the LGM lowstand, unconsolidated sediments deposited during regression were reworked and incorporated into coarse-grained beach deposits. At the onset of transgression, the lowstand subaerial delta transitioned into a subaqueous delta, signaled by the deposition of steeply dipping

foreset beds. Sample NA-075-115, collected immediately above our mapped LGM transgressive surface, is composed of silts and fine sand (muds were lost during suction sampling), and it contained two bivalves younger than the LGM (from early MIS 1 and late MIS 2), as well as one bivalve we presume to have been reworked (MIS 3 Table 5). The taxa in this sample restrict the minimum depth of deposition of this sample to ~50 m, consistent with deposition during transgression. In cross section, a lowstand subaerial delta is concave up at its base, due to the shape of the underlying clinoform layout, and convex up on its top, due to sediment diffusion at the top of the most distal foresets. These lozenge-shaped packages of sediment are often acoustically transparent and occasionally have negative impedance with respect to overlying deposits. The final transition from low dips (<6°) of subaerial deltas to high dips (6°–27°) of subaqueous deltas is the transgressive surface (Figs. 4B and 4D). During deposition throughout transgression, sediments deposited during the previous regression are partially eroded, and that material is redeposited in gradually deepening water. When sea level reaches a stable highstand, subaerial and subaqueous deltas are respectively deposited at depths of 0–15 m and 30–60 m (possibly deeper). The lowstand shelf becomes isolated from clastic sedimentation, and carbonate marls begin to form on the shelf.

### Potential Arguments Against Subsidence

Islands in the California Continental Borderland that are indisputably uplifting (e.g., San Nicolas [Muhs et al., 2014] and San Clemente [Muhs, 1982]) generally possess one subsided terrace approximately at lowstand sea level (Fig. S1 [see footnote 1]). A claim that San Clemente exhibits at least four subsided marine terraces has been taken to suggest that “the existence of terrace-like landforms around Santa Catalina Island does not necessarily constitute evidence of Quaternary subsidence” (Schumann et al., 2012, p. 220). However, the identification of these terraces around San Clemente Island is based on bathymetric data with gridding artifacts (Schumann et al., 2012, their fig. 12; cf. Fig. S1 herein [footnote 1]). Our incorporation of additional bathymetric data (Fig. S1 [footnote 1]) makes it clear that San Clemente is circumscribed by a single terrace, the outer edge of which was likely a subaqueous delta during the LGM lowstand, and that San Clemente exhibits no terraces >50 m below lowstand depth. Santa Cruz Island, although uplifting, is an exception in having some subsided terraces below lowstand depths, despite its recent and ongoing uplift (Pinter et al., 2001, 2003).

However, whereas Santa Catalina’s terraces and the single LGM terrace completely encircle that island, the subsided terraces around Santa Cruz Island (and Anacapa to the east and Santa Rosa Island to the west) only occur north and south of the islands and are the subsiding flanks of a growing anticline that is striking east-west. Pinter et al. (2003) showed that their conceptual model of Santa Cruz as a broad flexural “listric-thrust fold” is consistent with regional estimates of elastic thickness of just 4–8 km (Bechtel et al., 1990). We can rule out the possibility that Santa Catalina has similarly experienced onshore Quaternary uplift while surrounding terraces subsided using the same two-dimensional elastic-plate flexural model (Sandwell, 2001) as employed by previous researchers (e.g., Pinter et al., 2003). If Santa Catalina was uplifting while its terraces were subsiding, then the hinge line of zero-vertical motion must encircle the island between the coast and the first subsided terrace T3. A flexural wavelength equivalent to the maximum across-island distance between the hinge lines of ~15 km along section A-A’ and only ~6 km along section B-B’ (Fig. 2) would require elastic thicknesses of ~500 m and ~85 m, respectively, i.e., one or two orders of magnitude smaller than other estimates of elastic thickness on and offshore southern California (Sheffels and McNutt, 1986; Bechtel et al., 1990). Hence, it is implausible that Santa Catalina Island is uplifting while its terraces subside.

Additional evidence that Santa Catalina Island is not folding is the fanning of terrace dips to the northeast (Fig. 9) and the asymmetry of the drainage divide (Schumann et al., 2012), both of which are consistent with block tilting. The absence of onshore seismicity further suggests Catalina Ridge is a single block, bounded by near-vertical strike-slip faults, as shown by offshore seismicity and MCS profiles (Legg et al., 2015, their figs. 5C and 6B). The evidence of terrace subsidence around Santa Catalina and the evidence against significant internal deformation of the island block suggest that the interior of Santa Catalina is subsiding and tilting at the same rate as the offshore regions.

Having shown that islands in the California Continental Borderland that are marked with uplifted terraces have only a single subsided terrace (e.g., San Clemente), unless they are actively folding (e.g., Santa Cruz, Anacapa), and that Santa Catalina is tilting not folding, we are left with one final possibility for modern uplift of Santa Catalina. If the observed subsided terraces are all Early Pleistocene, then Late Pleistocene uplift is a theoretical possibility. Schumann et al. (2012) argued that the entirety of Santa Catalina Island, including its expected prominent MIS 5 terrace, has been

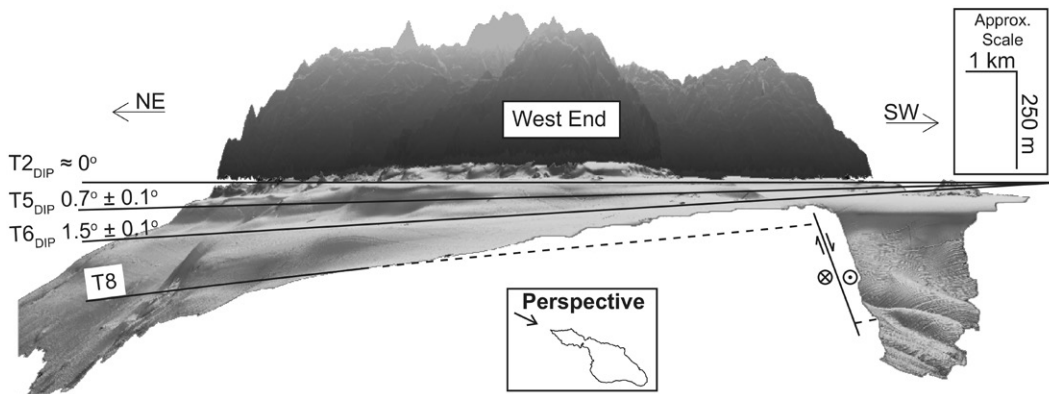


**Figure 9.** Three-dimensional (3-D) view of Santa Catalina and adjacent shelf looking southeast at North Point with 10× vertical exaggeration. Topography shown in dark gray, and higher elevations have “mist.” Bathymetry is represented in 3-D perspective view by digital elevation model (DEM; Fig. 2) overlain with slope map. Darker colors are steeper slopes. Subhorizontal lines are measured dips of terraces T2, T5, and T6, and dissected T8.

resurfaced by a pulse of “late Quaternary” uplift that has removed all early Pleistocene terraces. However the surface of the island’s interior is covered entirely with mature soils (USDA, 2008). The conglomerate at the Ben Weston Overlook (Fig. 2, red circle) contains rounded cobbles of garnet-amphibolite-facies Catalina Schist, which only outcrops near the airport (Grove et al., 2008, their fig. 2, red outline), and thus must have been transported southwest at least 5 km. Modern drainages between the garnet-amphibolite bedrock outcrops and the garnet-amphibolite cobble conglomerate strike roughly N60°W and do not allow garnet-amphibolite rocks from near the center of the island to be deposited at the Ben Weston Overlook today. This implies that a separate network of drainages predated the drainage network observed today, consistent with the interior topography of Santa Catalina having been formed by erosion over at least the 1.1 m.y. that we propose below as the latest possible onset of subsidence. Over the same time period, the steep topography near the coast was created by subsidence-induced coastal retreat that removed the alluviated canyons (often seen as a response to rising base level), producing topography that superficially appears uplifted.

#### Dating the Vertical Motion of Santa Catalina Island

Late Quaternary subsidence of Santa Catalina Island following uplift of Catalina Ridge is confirmed by multiple lines of evidence—most simply by faunal assemblages deposited in water shallower than 50 m that are now found at depths up to 350 m (Fig. 8). Identification of regressive through transgressive strata within each terrace provides a depositional model for the formation of submerged marine terraces during sea-level fluctuations, and it allows us to identify paleo-sea level. Samples above and be-

low our mapped transgressive surface within the 90 m terrace at Santa Catalina Island have radiocarbon ages consistent with our assignment of an LGM age. Our biostratigraphic evidence of the age of the deepest terrace sediments (extinct taxa in Fig. 8) provides only modest constraints on the timing of the onset of subsidence. Nonetheless, the presence of 16 successive parasequences (Fig. 5, profile 2202), each representing one fourth-order Milankovitch-scale sea-level cycle, requires subsidence over at least 16 sea-level cycles. Thus, the youngest possible age for the deepest sequence and the onset of subsidence is 1.13 Ma (MIS 34; Fig. 10; Lisiecki and Raymo, 2005).

Santa Catalina’s terrace package reaches a maximum depth of at least 470 m north of the island (Fig. 5, profile 2202), and the deepest subaerial/subaqueous delta transition identified is at  $408 \pm 2$  m depth, overlain by 15 additional parasequences. Following Lajoie (1986), we connected the modern depth of each subaerial/subaqueous delta transition to a corresponding lowstand in the sea-level curve with a straight line representing constant subsidence rate (Fig. 10A). Because the suite of parallel lines of con-

stant subsidence rate intersects all the principal lowstands in the paleo-sea-level curve (within uncertainties in the paleo-sea-level curve back to MIS 34), we suggest an average subsidence of 0.27 mm/yr for profile 2202 (Fig. 9A). Unconformities may be present that would require a lower average subsidence rate over a longer time period, but our correlation has the merit of explaining the existence of all 16 parasequences without changing the sign of vertical tectonic motion and with minimal variation in rate of deposition (i.e., no hiatuses). North of Avalon (Fig. 5, profile 2610), the deepest subaerial/subaqueous delta transition is at a depth of 290 m today, but it is also overlain by 15 parasequences, implying 195 m subsidence over 1.13 m.y. at 0.17 mm/yr. South of Avalon, terrace deposits become too thin to correlate, so we could not directly calculate a subsidence rate. However, the presence of the sequences at depths much greater than lowstand depth requires subsidence for this portion of the island also.

In contrast to the deep terraces northeast of the island, terraces along the Catalina Escarpment southwest of the island are consistently

**Figure 10 (on following page).** Correlation of submerged subaerial/subaqueous delta transitions with a glacial isostasy-adjusted (GIA) sea-level curve. Solid black line repeated in parts A, B, and C is the stacked sea-level record (Spratt and Lisiecki, 2015), adjusted for glacial isostasy using a lowstand value of ~95 m (Muhs et al., 2014). Dashed black line is a stack of 57 globally distributed benthic foraminiferal  $\delta^{18}\text{O}$  records (Lisiecki and Raymo, 2005), scaled to sea-level maxima and minima. Open circles on left side are subaerial/subaqueous delta transitions identified in seismic data (Figs. 5 and 6). Marine isotope stages (MIS) are shown along bottom, where gray time intervals correspond to gray-shaded subaerial/subaqueous deltas in Figures 5 and 6. Dipping lines are best-fit correlations of the subaerial/subaqueous delta transitions to stillstands in the GIA curve, using a constant subsidence rate. LGM—Last Glacial Maximum. (A) Stanford profile 2202, northeast of Santa Catalina, subsiding 0.27 mm/yr. (B) Stanford profile 2401, southeast of Santa Catalina, subsiding only 0.08 mm/yr, indicative of tilt to the northeast (Fig. 9). (C) Stanford profile 2103, across Pilgrim Banks, modeled as subsiding at 0.3 mm/yr back to 360 ka B.P., but at 0.12 mm/yr in the Middle Pleistocene.

Late Quaternary subsidence of Santa Catalina Island from submerged marine terraces

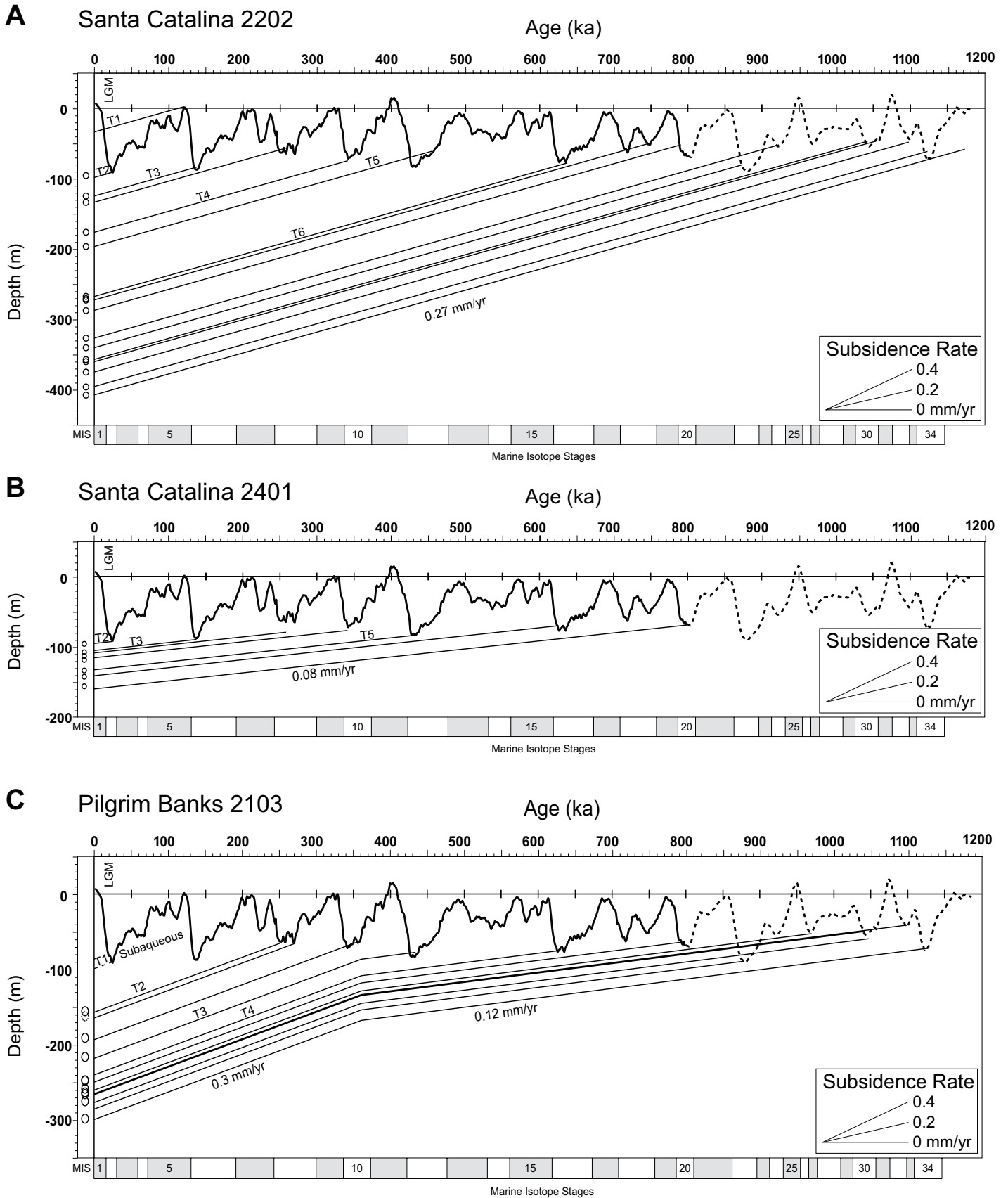
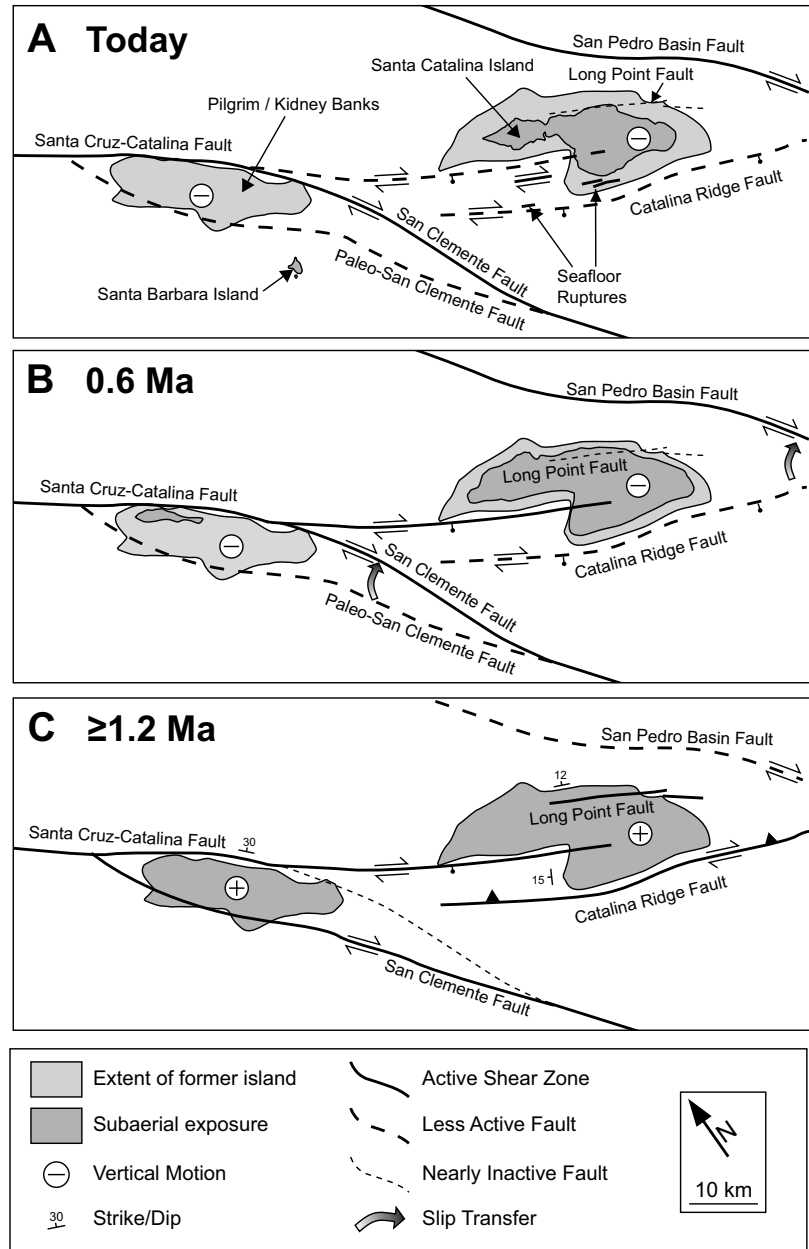


Figure 10.

thinner and fewer in number. South of Two Harbors (Fig. 5, profile 2503), the terraces contain seven identifiable parasequences, implying deposition since at least 0.8 Ma (MIS 20; Fig. 10B). The deepest observed subaerial/subaqueous delta transition on profile 2503 is now at a depth of ~160 m, implying subsidence of at least 65 m at ~0.08 mm/yr. South of Farnsworth Bank, the determination of a subsidence rate was complicated by active extension along the Catalina fault that forms the Catalina Escarpment (Fig. 2) and dissects the older terraces. The remaining thin terrace packages were correlated to T1–T6 on the NE side of the island, but any deeper terraces have been dissected by the Catalina fault and translated downslope and to the northwest. The fanned dips of T1–T6 on the northeast side of the island suggest NE tilting has accompanied subsidence. Bathymetric analysis (Keneally, 2016) showed that the deepest bathymetric terrace we can correlate around Santa Catalina Island (T6) dips ~1.5° to the northeast (Fig. 9), implying accumulated tilt of 1.5° since 625 ka (MIS 16). The deepest terraces overlie subplanar acoustic basement on an unconformity that dips ~3° to the northeast (Fig. 5, profiles 2610, 2202). If this basement was wave-planed, NE tilting likely predated, and then continued during, subsidence of Santa Catalina Island.

The Miocene to early Pliocene sedimentary rocks around Santa Catalina Island also provide constraints on the maximum uplift and the subaerial extent of the island at its Pliocene zenith. In most of our seismic profiles around northeast Santa Catalina Island, the terrace package unconformably overlies the contact between igneous-metamorphic basement (Fig. 2, dashed orange line; Fig. 5, profiles 2610, 2202 unconformity; Fig. 11C, gray area) and presumably Miocene sediments (Fig. 5, profiles 2610, 2202). The Miocene sediments are truncated at a surface that dips <5° seaward around the entire island. The contact between Miocene sediments and underlying basement (Fig. 11C, outline of gray area) has a roughly 1.5°N dip, consistent with the tilting direction of the island. This Miocene-basement contact is overlain by the distal portion of marine-terrace sediments around most of the island, except along the Catalina Escarpment, where marine-terrace sediments are truncated by the Santa Cruz–Catalina Ridge and Catalina faults. In map view, this contact has roughly the same shape as the terrace package that overlies it, and it crudely marks the maximum subaerial extent of Santa Catalina Island before subsidence, i.e., roughly 3× its current area. Thus, Santa Catalina Island has had roughly the same shape for at least 1 m.y. (Fig. 11C).



**Figure 11. Fault organization and island configuration as suggested by vertical-motion indicators of the subsided marine terraces: (A) today; (B) at 0.6 Ma; and (C) at ca. 1.2 Ma. Note figure orientation, with northeast-up orientation.**

### Vertical Motion of the Pilgrim/Kidney Banks

The Pilgrim Banks terrace package contains 13 successive sequence boundaries, and possibly many more that cannot be counted due to dissection by the Santa Cruz–Catalina Ridge fault. Chaytor et al. (2008) showed that the Pilgrim/Kidney Banks have tilted slightly to the northwest (<1°), possibly due to their underthrusting beneath the Western Transverse Ranges at the Channel Islands thrust (Fig. 1).

Our seismic profiles crossing the Pilgrim/Kidney Banks perpendicular to the direction of this tilt show that terrace back-edges on the southwest and northeast sides of the bank are at nearly equal elevations (Fig. 6, 2103, dashed lines). Due to their proximity, Santa Catalina Island and Pilgrim Banks have experienced similar weather systems, oceanographic conditions, and sea-level history. Hence, we can correlate the terraces at Santa Catalina Island and Pilgrim Bank based on stratigraphic similarity between both platforms, in particular similar-

ity of the MIS14/16 forced regressive wedge (Fig. 5, 2202, 2610; Fig. 6, 2103). This correlation allows us to match sequences back to 1.15 Ma (MIS 34; Fig. 10C), and it suggests that the deepest subaerial/subaqueous delta transition at Pilgrim Banks, now at ~300 m depth, has been subsiding for 1.15 m.y. We could find no correlation between modern depths of delta transitions and the paleo–sea-level curve that permitted a constant subsidence rate, and our data are best fit by an increase in subsidence from ~0.12 mm/yr to ~0.3 mm/yr at 400–350 ka (Fig. 10C). The larger Kidney Banks platform is surrounded on most sides by an intermittent terrace package that is too thin to permit detailed analysis or correlation to the Santa Catalina Island terrace package. However, no major tectonic break has been identified between Pilgrim and Kidney Banks, and we suggest that they subsided together, with Pilgrim Banks being the last remnant of a once-larger island (~270 km<sup>2</sup>; Fig. 11C) that became submerged (during sea-level highstands) by ca. 0.5 Ma (Fig. 11B).

### Causes of Vertical Tectonic Motions in the California Continental Borderland

The late Miocene subsidence, Pliocene uplift, and post–mid-Pleistocene subsidence of Santa Catalina Island and the Pilgrim/Kidney Banks require multiple causes. The early Miocene clockwise rotation of the Western Transverse Ranges away from the Peninsular Ranges (Luyendyk et al., 1985) and eruption of voluminous volcanics created a proto–Santa Catalina Island (Legg, 1991; Crouch and Suppe, 1993). The contemporaneous extreme rifting of the Inner Borderland set the stage for late Miocene thermal subsidence (Turcotte and McAadoo, 1979) and accommodation of the Monterey Formation. However, the maximum thermal subsidence rate today, 15 m.y. after cessation of rifting, should be only ~0.05 mm/yr, based on the oceanic–lithosphere depth–age curve (Parsons and Sclater, 1977), which is far slower than the subsidence rates we demonstrate in this paper (up to 0.3 mm/yr; Fig. 10). In contrast, isostatic subsidence would likely be far faster than we observe, because Maxwell relaxation times estimated from glacio–isostatic rebound are short (0.0001–0.1 m.y.; Adams et al., 1999; Dixon et al., 2004) compared to the ≥1 m.y. duration of subsidence of Santa Catalina Island and the Pilgrim/Kidney Banks.

We propose that the dominant control on uplift and subsidence of the Inner Borderland since Miocene time has been changes in the linkages of the anastomosing faults that are part of the greater San Andreas transform plate boundary. The most recent uplift of the Santa Cruz–Cata-

lina Ridge began by earliest Pliocene, probably when the Pacific–North America plate boundary jumped inland from the Inner Borderland at ca. 6 Ma (Stock and Hodges, 1989). Transpression along reactivated Miocene extensional structures has been suggested as a mechanism for the uplift of Santa Catalina Island, and it is documented in folded Miocene sedimentary rocks on the southwest margin of the Santa Cruz–Catalina Ridge (Legg et al., 2004a; Francis et al., 2018). A regional stress field seems to be required to explain the simultaneous uplift of the Pilgrim Banks and Santa Catalina Island on opposite sides of the Santa Cruz–Catalina Ridge fault (Fig. 11C), and we presume that the entire Santa Catalina–Pilgrim Banks region was in transpression during Pliocene time due to the obliquity of the Santa Cruz–Catalina Ridge fault and the paleo–San Clemente fault to the relative plate–motion vector between the Pacific and North American plates (Fig. 1).

Our images of terrace sedimentary packages require subsidence since older than 1 Ma, and they also document continuous, albeit modest extension across the Catalina fault for most of this period (Fig. 11B). Profile 2503 (Figs. 4 and 5) shows a normal–sense growth fault that clearly offsets the basement unconformity by ~20 m, and it also shows evidence of rupture at the seafloor (Fig. 2, inset 1; Fig. 11A). Comparison with profile 2401 (Figs. 5 and 10B) suggests that the deepest offset terrace package was deposited in MIS 20, at ca. 800 ka, providing a minimum age for the onset of faulting. We propose that the transition from uplift to subsidence was triggered by a reduction of motion along the restraining segment of the Catalina fault and increased slip on the southern San Pedro Basin fault northeast of Santa Catalina (Fig. 11A; Francis et al., 2018), thereby allowing Santa Catalina Island to subside. The active Santa Cruz–Catalina Ridge fault zone continues to suppress subsidence southwest of Santa Catalina Island, while on the northeast side, subsidence continues due to sedimentary loading on the flanks of the San Pedro and Santa Monica Basins, thereby accounting for the observed tilting of the island to the northeast. The subsidence of Pilgrim Banks may represent a similar transfer of slip from the San Clemente fault (Legg, 1991), which runs west of the Pilgrim/Kidney Banks, to the active East San Clemente fault where it merges with the Santa Cruz–Catalina Ridge fault.

### CONCLUSIONS

New high-resolution seismic-reflection and paleontological data show that the terrace package surrounding Santa Catalina Island

contains at least 16 successive transgressive–regressive sequences, requiring at least 16 sea-level cycles and indicating a minimum age of 1.15 Ma. Sediments recovered during ROV dives from subsided marine terraces, offshore Avalon, Santa Catalina Island, contain several extinct Pliocene to Middle Pleistocene shallow-water taxa confirming Quaternary subsidence. The entirety of Santa Catalina Island has subsided between 0.08 and 0.27 mm/yr for at least 1.15 m.y., and tilted north at least 1.5° during this time. Pilgrim Banks has a similar succession of subsided terraces that we correlate to the terraces near Santa Catalina Island, yet it requires a variable subsidence rate to explain their depth distribution. We estimate that the Pilgrim Banks area has been subsiding at 0.3 mm/yr for at least 0.35 m.y. but must have subsided no faster than 0.12 mm/yr between 1.15 and 0.35 Ma. The subsided terraces in the Inner Borderland contain a detailed record of lowstands and interstadials during the Quaternary that, with more precise determination of subsidence rates, will provide valuable constraints on paleo–sea level and ultimately glacial ice volume and distribution. Even at the present state of knowledge, the essentially uniform subsidence rate for Santa Catalina Island that we demonstrate here must finally settle the century-old feud between subsidors and uplifters in favor of Quaternary subsidence.

### DATA AVAILABILITY

ROV samples NA067-001–NA067-021 are archived at the Graduate School of Oceanography, University of Rhode Island. Grab samples and all fossils described in this paper are stored at Stanford University. Digital versions of the migrated seismic data and bathymetric compilations shown in this paper are available from the Stanford Digital Repository, <https://purl.stanford.edu/sk175bh2032>.

### ACKNOWLEDGMENTS

The E/V *Nautilus* and the Ocean Exploration Trust conducted ROV sampling and acquired bathymetric coverage at and around Santa Catalina Island and Pilgrim Banks in cruises led by Mike Brennan and Nicole Raineault. Other bathymetric data used in this study were acquired, processed, and distributed by the Seafloor Mapping Laboratory, California State University–Monterey Bay, or were sourced from the National Oceanic and Atmospheric Administration (NOAA) National Center for Environmental Information (formerly NGDC). Seismic processing was completed using OpenCPS™ tools donated by Open Geophysical, Inc. (now part of Shearwater Geoservices AS). We thank Theory Marine Services, Captain Brayton Pointner, the Southern California Marine Institute, Captain Dennis Dunn, and the crew of R/V *Yellowfin*. Kingdom Suite software was available thanks to a generous grant from IHS Markit™ to California State University–Long Beach and Stanford University. California State University–Long Beach seismic surveys and analysis were supported by a grant from the American Chemical Society Petro-

leum Research Fund. Stanford University seismic surveys were supported by Conoco-Phillips, Inc., by the Southern California Earthquake Center (SCEC) grants 15149 and 16097, and by equipment loans from Geometrics (San Jose, California), and Subsea Systems (Ventura, California) through Mike Barth. Danny Brothers and George Tate at the U.S. Geological Survey Pacific Coastal Marine Science Center facilitated the loan of coring and grab-sampling equipment. Radiocarbon age analyses funded by SCEC were obtained at the Lawrence Livermore National Laboratory Center for Accelerator Mass Spectrometry, managed by Tom Guilderson. Lynn Dodd (University of Southern California) and Wendy Teeter (University of California–Los Angeles) provided assistance with onshore logistics and field work. Valuable discussions with Stephan Graham, Marty Grove, Tim McHargue, and George Hilley contributed to this study. Portions of the bathymetric and seismic data were interpreted by Ian Keneally and Ethan Williams as part of their senior and honor's theses at Stanford University. Castillo was also supported by a National Science Foundation Graduate Fellowship. Conni De Masi Castillo assisted with photography.

#### REFERENCES CITED

- Adams, K.D., Wesnousky, S.G., and Bills, B.G., 1999, Isostatic rebound, active faulting, and potential geomorphic effects in the Lake Lahontan basin, Nevada and California: *Geological Society of America Bulletin*, v. 111, p. 1739–1756, [https://doi.org/10.1130/0016-7606\(1999\)111<1739:IRAFAP>2.3.CO;2](https://doi.org/10.1130/0016-7606(1999)111<1739:IRAFAP>2.3.CO;2).
- Alexander, C.R., DeMaster, D.J., and Nittrouer, C.A., 1991, Sediment accumulation in a modern epicontinental-shelf setting: The Yellow Sea: *Marine Geology*, v. 98, p. 51–72, [https://doi.org/10.1016/0025-3227\(91\)90035-3](https://doi.org/10.1016/0025-3227(91)90035-3).
- Argow, B.A., 1999, Benthic foraminiferal biofacies across a high energy continental shelf, San Onofre, California [M.S. thesis]: Stanford, California, Stanford University, 207 p.
- Atwater, T., 1970, Implications of plate tectonics for the Cenozoic tectonic evolution of western North America: *Geological Society of America Bulletin*, v. 81, p. 3513–3536, [https://doi.org/10.1130/0016-7606\(1970\)81\[3513:IOPTFT\]2.0.CO;2](https://doi.org/10.1130/0016-7606(1970)81[3513:IOPTFT]2.0.CO;2).
- Bandy, O.L., 1963, Dominant paralic foraminifera of southern California and the Gulf of California: *Contributions from the Cushman Foundation for Foraminiferal Research*, v. 14, p. 127–134.
- Bandy, O.L., Ingle, J.C., and Resig, J.M., 1964, Facies trends, San Pedro Bay, California: *Geological Society of America Bulletin*, v. 75, p. 403–424, [https://doi.org/10.1130/0016-7606\(1964\)75\[403:FTSPBC\]2.0.CO;2](https://doi.org/10.1130/0016-7606(1964)75[403:FTSPBC]2.0.CO;2).
- Bechtel, T.D., Forsyth, D.W., Sharpton, V.L., and Grieve, R.A., 1990, Variations in effective elastic thickness of the North American lithosphere: *Nature*, v. 343, p. 636–638, <https://doi.org/10.1038/343636a0>.
- Bell, K.L.C., Brennan, M.L., Flanders, J., Raineault, N.A., and Wagner, K., eds., 2016, New frontiers in ocean exploration: The E/V *Nautilus* and NOAA Ship *Okeanos Explorer* 2015 field season: *Oceanography*, v. 29, no. 1, supplement, 84 p., <https://doi.org/10.5670/oceanog.2016.supplement.01>.
- Bryant, M.E., 1987, Emergent marine terraces and Quaternary tectonics: Palos Verdes Peninsula, California, in Fischer, P.J., ed., *Geology of the Palos Verdes Peninsula and San Pedro Bay*: Los Angeles, California, Pacific Section, Society of Economic Paleontologists and Mineralogists (SEPM), p. 63–78.
- Chaytor, J.D., Goldfinger, C., Meiner, M.A., Huftile, G.J., Romsos, C.G., and Legg, M.R., 2008, Measuring vertical tectonic motion at the intersection of the Santa Cruz–Catalina Ridge and northern Channel Islands platform, California Continental Borderland, using submerged paleoshorelines: *Geological Society of America Bulletin*, v. 120, p. 1053–1071, <https://doi.org/10.1130/B26316.1>.
- Chiocci, F.L., and Orlando, L., 1996, Lowstand terraces on Tyrrhenian Sea steep continental slopes: *Marine Geology*, v. 134, p. 127–143, [https://doi.org/10.1016/0025-3227\(96\)00023-0](https://doi.org/10.1016/0025-3227(96)00023-0).
- Coan, E.V., Valentich-Scott, P., and Bernard, F.R., 2000, Bivalve seashells of western North America: Marine bivalve mollusks from Arctic Alaska to Baja California, in *Studies in Biodiversity*, volume 2: Santa Barbara Museum of Natural History Monograph no. 2, 764 p.
- Cooper, W.C., 1961, Natural foraminifera of the California and Oregon coast: *Contributions from the Cushman Foundation for Foraminiferal Research*, v. 12, p. 47–63.
- Crouch, J.K., and Suppe, J., 1993, Late Cenozoic tectonic evolution of the Los Angeles Basin and Inner California Borderland—A model for core complex–like crustal extension: *Geological Society of America Bulletin*, v. 105, p. 1415–1434, [https://doi.org/10.1130/0016-7606\(1993\)105<1415:LCTEOT>2.3.CO;2](https://doi.org/10.1130/0016-7606(1993)105<1415:LCTEOT>2.3.CO;2).
- Darling, K.F., Kucera, M., Kroon, D., and Wade, C.M., 2006, A resolution for the coiling paradox in *Neogloboquadrina pachyderma*: *Paleoceanography*, v. 21, PA2011, <https://doi.org/10.1029/2005PA001189>.
- Davis, J.C., Proctor, I.D., Southon, J.R., Caffee, M.W., Heikkinen, D.W., Roberts, M.L., Moore, T.L., Turlentaub, K.W., Nelson, D.E., Loyd, D.H., and Vogel, J.S., 1990, LLNL/UC AMS facility and research program: Nuclear Instruments Methods in Physics Research, Section B, no. B52, p. 269–272.
- Davis, P., 2004, The marine terrace enigma of Catalina Island—An uplifting experience?, in Legg, M., Davis, P., and Gath, E., eds., *Geology and Tectonics of Santa Catalina Island and the California Continental Borderland*: Santa Ana, California, South Coast Geological Society, Field Trip Guidebook 32, p. 115–122.
- Dixon, J.E., Dixon, T.H., Bell, D.R., and Malservisi, R., 2004, Lateral variation in upper mantle viscosity: Role of water: *Earth and Planetary Science Letters*, v. 222, p. 451–467, <https://doi.org/10.1016/j.epsl.2004.03.022>.
- Douglas, R.G., 1981, Paleocology of continental margin basins: A modern case history from the borderland of southern California, in Douglas, R.G., Colburn, I.P., and Gorsline, D.S., eds., *Depositional Systems in Active Continental Margin Basins*: Los Angeles, California, Pacific Section, Society of Economic Paleontologists and Mineralogists (SEPM), Short Course Notes, p. 121–156.
- Douglas, R.G., Liestman, J., Walch, C., Blake, G., and Cotton, M.L., 1980, The transition from live to sediment assemblage in benthic foraminifera from the southern California borderland, in Field, M.E., Bouma, A.H., and Colburn, I.P., eds., *Quaternary Depositional Environments from the Pacific Coast*: Los Angeles, California, Pacific Section, Society of Economic Paleontologists and Mineralogists (SEPM), Pacific Coast Paleogeography Symposium 4, p. 257–280.
- Emery, K.O., 1958, Shallow submerged terraces off southern California: *Geological Society of America Bulletin*, v. 69, p. 39–60, [https://doi.org/10.1130/0016-7606\(1958\)69\[39:SSMTOS\]2.0.CO;2](https://doi.org/10.1130/0016-7606(1958)69[39:SSMTOS]2.0.CO;2).
- Francis, R.D., and Legg, M.R., 2010, Quaternary uplift and subsidence of Catalina Ridge and San Pedro Basin, Inner California Continental Borderland, offshore southern California: Results of high-resolution seismic profiling: San Francisco, California, American Geophysical Union, Fall Meeting supplement, abstract T13C–2218.
- Francis, R.D., Legg, M.R., and Castillo, C.M., 2018, Shear zone faulting, volcanism, and basin evolution along a continental margin transform system: San Pedro Basin, offshore Southern California, in Schwabach, J.R., Marsaglia, K.M., and Behl, R.J., eds., *From the Mountains to the Abyss: The California Borderland as an Archive of Southern California Geologic Evolution*: Society for Sedimentary Geology (SEPM) Special Publication 110, <https://doi.org/10.2110/sepm.sp.110.113>.
- Galloway, J.J., and Wissler, S.G., 1927, Pleistocene foraminifera from the Lomita Quarry, Palos Verdes Hills, California: *Journal of Paleontology*, v. 1, p. 35–87.
- Glassow, M.A., 1980, Recent developments in the archaeology of the Channel Islands, in Powell, D.M., ed., *The California Islands: Proceedings of a Multidisciplinary Symposium*: Santa Barbara, California, Santa Barbara Museum of Natural History, p. 79–99.
- Grant, L.B., Mueller, K.J., Gath, E.M., Cheng, H., Edwards, R.L., Munro, R., and Kennedy, G.L., 1999, Late Quaternary uplift and earthquake potential of the San Joaquin Hills, southern Los Angeles Basin, California: *Geology*, v. 27, p. 1031–1034, [https://doi.org/10.1130/0091-7613\(1999\)027<1031:LQUAEP>2.3.CO;2](https://doi.org/10.1130/0091-7613(1999)027<1031:LQUAEP>2.3.CO;2).
- Grove, M., Bebout, G.E., Jacobson, C.E., Barth, A.P., Kimbrough, D.L., King, R.L., Zou, H., Lovera, O.M., Mahoney, B.J., and Gehrels, G.E., 2008, The Catalina Schist: Evidence for Middle Cretaceous subduction erosion of southwestern North America, in Draut, A.E., Clift, P.D., and Scholl, D.W., eds., *Formation and Applications of the Sedimentary Record in Arc Collision Zones*: Geological Society of America Special Paper 436, p. 335–361, [https://doi.org/10.1130/2008.2436\(15\)](https://doi.org/10.1130/2008.2436(15)).
- Hauksson, E., and Jones, L., 1988, The July 1986 Oceanside (ML = 5.3) earthquake sequence in the continental borderland, southern California: *Bulletin of the Seismological Society of America*, v. 78, p. 1885–1906.
- Hendy, I.L., 2010, The paleoclimatic response of the Southern California margin to the rapid climate change of the last 60 ka: A regional view: *Quaternary International*, v. 215, p. 62–73, <https://doi.org/10.1016/j.quaint.2009.06.009>.
- Howell, D.G., and Vedder, J.G., 1981, Structural implications of stratigraphic discontinuities across the southern California borderland, in Ernst, W.G., ed., *The Geotectonic Development of California*, Rubey Volume 1: Englewood Cliffs, New Jersey, Prentice Hall, p. 535–558.
- Howell, D.G., Champion, D.E., and Vedder, J.G., 1987, Terrane accretion, crustal kinematics, and basin evolution, southern California, in Ingersoll, R.A., and Ernst, W.G., eds., *Cenozoic Basin Development of Coastal California*, Rubey Volume 6: Englewood Cliffs, New Jersey, Prentice Hall, p. 242–258.
- Hunt, D., and Tucker, M.E., 1992, Stranded parasequences and the forced regressive wedge systems tract: Deposition during base-level fall: *Sedimentary Geology*, v. 81, p. 1–9, [https://doi.org/10.1016/0037-0738\(92\)90052-S](https://doi.org/10.1016/0037-0738(92)90052-S).
- Ingram, B.L., and Southon, J.R., 1996, Reservoir ages in eastern Pacific coastal and estuarine waters: *Radiocarbon*, v. 38, no. 3, p. 573–582, <https://doi.org/10.1017/S003822200030101>.
- Jardine, W.G., 1981, The determination of former shoreline positions in areas of large tidal range, with examples taken mainly from Scotland: *Bulletin de l'Association Française pour l'Etude du Quaternaire*, v. 18–2, p. 67–70.
- Junger, A., 1979, Maps and seismic profiles showing geologic structure of the Northern Channel Islands platform, California Continental Borderland: U.S. Geological Survey Miscellaneous Field Studies Map MF-991, 3 maps + 16 p.
- Keen, A.M., 1971, Sea Shells of Tropical West America: Marine Mollusks from Baja California to Peru: Stanford, California, Stanford University Press, 1064 p.
- Keneally, I., 2016, Seismic sequence stratigraphic evaluation of western Santa Catalina Island [Honor's thesis]: Stanford, California, Department of Geophysics, Stanford University, 42 p.
- Kennett, J.P., and Venz, K., 1992, Late Quaternary climatically related planktonic foraminiferal assemblage changes: Hole 893A, Santa Barbara Basin, California, in Musgrave, R.J., Kennet, J.P., Baldauf, J.G., and Lyle, M., eds., *Proceedings of the Ocean Drilling Program, Scientific Results, Volume 146*: College Station, Texas, Ocean Drilling Program, p. 281–294, <http://www-odp.tamu.edu/publications/srv/abstr146B/146b-21.htm>.
- Kucera, M., and Kennett, J.P., 2000, Biochronology and evolutionary implications of late Neogene California margin planktonic foraminiferal events: *Marine Micropaleontology*, v. 40, p. 67–81, [https://doi.org/10.1016/S0377-8398\(00\)00029-3](https://doi.org/10.1016/S0377-8398(00)00029-3).
- Kuehl, S.A., DeMaster, D.J., and Nittrouer, C.A., 1986, Nature of sediment accumulation on the Amazon con-

## Late Quaternary subsidence of Santa Catalina Island from submerged marine terraces

- tinental shelf: *Continental Shelf Research*, v. 6, p. 209–225, [https://doi.org/10.1016/0278-4343\(86\)90061-0](https://doi.org/10.1016/0278-4343(86)90061-0).
- Lajoie, K.R., 1986, Coastal tectonics, in *Geophysics Study Committee, Geophysics Research Forum, Commission on Physical Sciences, Mathematics, and Applications, National Research Council, Division on Engineering and Physical Sciences, compiler, Active Tectonics: Impact on Society*: Washington, D.C., National Academy Press, p. 95–124, <http://books.google.com/books?hl=en&lr=&id=qaz9KnE2lxQC&pgis=1>.
- Lajoie, K.R., Ponti, D.J., Powell, C.L., Mathieson, S.A., and Sarna-Wojcicki, A.M., 1991, Emergent marine strandlines and associated sediments, coastal California: A record of Quaternary sea-level fluctuations, vertical tectonic movements, climatic changes, and coastal processes, in Morrison, R.B., ed., *Quaternary Nonglacial Geology: Conterminous U.S.*: Boulder, Colorado, Geological Society of America, The Geology of North America, v. K-2, p. 190–203.
- Lankford, R.R., and Phleger, F.B., 1973, Foraminifera from the nearshore turbulent zone, western North America: *Journal of Foraminiferal Research*, v. 3, p. 101–132, <https://doi.org/10.2113/gsjfr.3.3.101>.
- Lawson, A.C., 1894, The post-Pliocene diastrophism of the coast of southern California: *Bulletin of the Department of Geology, University of California*, v. 1, p. 15–160.
- Legg, M.R., 1991, Developments in understanding the tectonic evolution of the California Continental Borderland, in Osborne, R.H., ed., *From Shoreline to Abyss: Contributions in Marine Geology in Honor of Francis Parker Shepard*: Society for Sedimentary Geology (SEPM) Special Publication 46, p. 291–312, [http://archives.datapages.com/data/sepm\\_sp/SP46/Developments\\_in\\_Understanding.htm](http://archives.datapages.com/data/sepm_sp/SP46/Developments_in_Understanding.htm).
- Legg, M.R., Borrero, J.C., and Synolakis, C.E., 2004a, Tsunami hazards associated with the Catalina fault in southern California: *Earthquake Spectra*, v. 20, p. 917–950, <https://doi.org/10.1193/1.1773592>.
- Legg, M.R., Davis, P.M., and Gath, E.M., 2004b, Geology and Tectonics of Santa Catalina Island and the California Continental Borderland: Santa Ana, California, South Coast Geological Society, 409 p.
- Legg, M.R., Goldfinger, C., Kamerling, M.J., Chaytor, J.D., and Einstein, D.E., 2007, Morphology, structure and evolution of California Continental Borderland restraining bends, in Cunningham, W.D., and Mann, P., eds., *Tectonics of Strike-Slip Restraining and Releasing Bends*: Geological Society, London, Special Publication 290, p. 143–168, <https://doi.org/10.1144/SP290.3>.
- Legg, M.R., Kohler, M.D., Shintaku, N., and Weeraratne, D.S., 2015, High-resolution mapping of two large-scale transpressional fault zones in the California Continental Borderland: Santa Cruz–Catalina Ridge and Ferrelle faults: *Journal of Geophysical Research–Earth Surface*, v. 120, p. 915–942, <https://doi.org/10.1002/2014JF003322>.
- Lipps, J.H., 1967, Age and environment of a marine terrace fauna, San Clemente Island, California: *The Veliger*, v. 9, p. 388–398.
- Lipps, J.H., Valentine, J.W., and Mitchell, E., 1968, Pleistocene paleoecology and biostratigraphy, Santa Barbara Island, California: *Journal of Paleontology*, v. 42, p. 291–307.
- Lisiecki, L.E., and Raymo, M.E., 2005, A Pliocene–Pleistocene stack of 57 globally distributed benthic  $\delta^{18}\text{O}$  records: *Paleoceanography*, v. 20, p. 1003–1020, <https://doi.org/10.1029/2004PA001071>.
- Loop, T.H., 1973, Dissected marine terraces on Santa Catalina Island, California: *Journal of Sedimentary Research*, v. 43, p. 841–843, <https://doi.org/10.1306/74D72888-2B21-11D7-8648000102C1865D>.
- Luyendyk, B.P., Kamerling, M.J., Terres, R.R., and Hornafius, J.S., 1985, Simple shear of southern California during Neogene time suggested by paleomagnetic declinations: *Journal of Geophysical Research*, v. 90, p. 12,454–12,466, <https://doi.org/10.1029/JB090iB14p12454>.
- Lyle, M., Koizumi, I., Delaney, M.L., and Barron, J.A., 2000, Sedimentary record of the California current system, middle Miocene to Holocene: A synthesis of Leg 167 results, in Lyle, M., Koizumi, I., Richter, C., and Moore, T.C., eds., *Proceedings of the Ocean Drilling Program, Scientific Results, Volume 167*: College Station, Texas, Ocean Drilling Program, p. 341.
- McLean, J.H., and Groslinger, T.M., 1996, Taxonomic atlas of the benthic fauna of the Santa Maria Basin and western Santa Barbara Channel, Volume 9: The Mollusca Part 2: The Gastropoda: Santa Barbara Museum of Natural History, 228 p.
- McGann, M., 2002, Historical and modern distributions of benthic foraminifera on the continental shelf of Monterey Bay, California: *Marine Geology*, v. 181, p. 115–156, [https://doi.org/10.1016/S0025-3227\(01\)00264-X](https://doi.org/10.1016/S0025-3227(01)00264-X).
- McGann, M., 2009, Review of impacts of contaminated sediment on microfaunal communities in the Southern California Bight, in Lee, H.J., and Normark, W.R., eds., *Earth Science in the Urban Ocean: The Southern California Continental Borderland*: Geological Society of America Special Paper 454, p. 413–455, [https://doi.org/10.1130/2009.2454\(6.3\)](https://doi.org/10.1130/2009.2454(6.3)).
- McGlasson, R.H., 1959, Foraminiferal biofacies around Santa Catalina Island, California: *Micropaleontology*, v. 5, p. 217–240, <https://doi.org/10.2307/1484211>.
- Miall, A., 2010, *The Geology of Stratigraphic Sequences*: Berlin, Springer Science & Business Media, 522 p., <https://doi.org/10.1007/978-3-642-05027-5>.
- Mitchell, N.C., Masselink, G., Huthnance, J.M., Fernandez-Salas, L.M., and Lobo, F.J., 2012, Depths of modern coastal sand clinoforms: *Journal of Sedimentary Research*, v. 82, p. 469–481, <https://doi.org/10.2110/jsr.2012.40>.
- Moore, E.J., 1984, Tertiary Marine Pelecypods of California and Baja California: Propeamussiidae and Pectinidae: U.S. Geological Survey Professional Paper 1228-B, 112 p.
- Moore, E.J., 1992, Tertiary Marine Pelecypods of California and Baja California: Erycinidae through Carditidae: U.S. Geological Survey Professional Paper 1228-E, 67 p.
- Muhs, D.R., 1982, A soil chronosequence on Quaternary marine terraces, San Clemente Island, California: *Geoderma*, v. 28, p. 257–283, [https://doi.org/10.1016/0016-7061\(82\)90006-4](https://doi.org/10.1016/0016-7061(82)90006-4).
- Muhs, D.R., and Szabo, B.J., 1982, Uranium-series age of the Eel Point terrace, San Clemente Island, California: *Geology*, v. 10, p. 23–26, [https://doi.org/10.1130/0091-7613\(1982\)10<23:UAOTEP>2.0.CO;2](https://doi.org/10.1130/0091-7613(1982)10<23:UAOTEP>2.0.CO;2).
- Muhs, D.R., Rockwell, T., and Kennedy, G., 1992, Late Quaternary uplift rates of marine terraces on the Pacific coast of North America, southern Oregon to Baja California Sur: *Quaternary International*, v. 15/16, p. 121–133, [https://doi.org/10.1016/1040-6182\(92\)90041-Y](https://doi.org/10.1016/1040-6182(92)90041-Y).
- Muhs, D.R., Simmons, K.R., Schumann, R.R., Groves, L.T., DeVogel, S.B., Minor, S.A., and Laurel, D., 2014, Coastal tectonics on the eastern margin of the Pacific Rim: Late Quaternary sea-level history and uplift rates, Channel Islands National Park, California, USA: *Quaternary Science Reviews*, v. 105, p. 209–238, <https://doi.org/10.1016/j.quascirev.2014.09.017>.
- Niemi, N.A., Oskin, M., and Rockwell, T.K., 2008, Southern California Earthquake Center geologic vertical motion database: *Geochemistry Geophysics Geosystems*, v. 9, Q07010, <https://doi.org/10.1029/2008GC002017>.
- Parsons, B., and Sclater, J.G., 1977, An analysis of the variation of ocean floor bathymetry and heat flow with age: *Journal of Geophysical Research*, v. 82, p. 803–827, <https://doi.org/10.1029/JB082i005p0803>.
- Passaro, S., Ferranti, L., and de Alteriis, G., 2011, The use of high-resolution elevation histograms for mapping submerged terraces: Tests from the eastern Tyrrhenian Sea and the eastern Atlantic Ocean: *Quaternary International*, v. 232, p. 238–249, <https://doi.org/10.1016/j.quaint.2010.04.030>.
- Patruno, S., Hampson, G.J., and Jackson, C.A.L., 2015, Quantitative characterisation of deltaic and subaqueous clinoforms: *Earth-Science Reviews*, v. 142, p. 79–119, <https://doi.org/10.1016/j.earscirev.2015.01.004>.
- Patterson, R.T., Brunner, C.A., Capo, R., and Dahl, J., 1990, A paleoenvironmental study of early to middle Pleistocene foraminifera of the Santa Barbara Formation at Santa Barbara, California: *Journal of Paleontology*, v. 64, p. 1–25, <https://doi.org/10.1017/S0022336000042190>.
- Pedoja, K., Husson, L., Regard, V., Cobbold, P.R., Ostancaux, E., Johnson, M.E., Kershaw, S., Saillard, M., Martinod, J., Furgerot, L., Weill, P., and Delcaillau, B., 2011, Relative sea-level fall since the last interglacial stage: Are coasts uplifting worldwide?: *Earth-Science Reviews*, v. 108, p. 1–15, <https://doi.org/10.1016/j.earscirev.2011.05.002>.
- Pinter, N., Johns, B., Little, B., and Vestal, W.D., 2001, Fault-related folding in California's northern Channel Islands documented by rapid-static GPS positioning: *GSA Today*, v. 11, no. 5, p. 4–9, [https://doi.org/10.1130/1052-5173\(2001\)011<0004:FRFICN>2.0.CO;2](https://doi.org/10.1130/1052-5173(2001)011<0004:FRFICN>2.0.CO;2).
- Pinter, N., Sorlien, C.C., and Scott, A.T., 2003, Fault-related fold growth and isostatic subsidence, California Channel Islands: *American Journal of Science*, v. 303, p. 300–318, <https://doi.org/10.2475/ajs.303.4.300>.
- Pirmez, C., Pratson, L.F., and Steckler, M.S., 1998, Clinoform development by advection-diffusion of suspended sediment: Modeling and comparison to natural systems: *Journal of Geophysical Research*, v. 103, p. 24,141–24,157, <https://doi.org/10.1029/98JB01516>.
- Platt, J.P., 1976, The significance of the Catalina Schist in the history of the southern California borderland, in Howell, D.G., ed., *Aspects of the Geologic History of the California Continental Borderland: Pacific Section, American Association of Petroleum Geologists, Miscellaneous Publication 24*, p. 47–52.
- Pomar, L., and Tropeano, M., 2001, The Calcarene di Gravina Formation in Matera (southern Italy): New insights for coarse-grained, large-scale, cross-bedded bodies encased in offshore deposits: *American Association of Petroleum Geologists Bulletin*, v. 85, p. 661–690.
- Reimer, P.J., Bard, E., Bayliss, A., Beck, J.W., Blackwell, P.G., Ramsey, C.B., Buck, C.E., Cheng, H., Edwards, R.L., Friedrich, M., and Grootes, P.M., 2013, IntCal13 and Marine13 radiocarbon age calibration curves 0–50,000 years cal BP: *Radiocarbon*, v. 55, no. 4, p. 1869–1887, [https://doi.org/10.2458/azu\\_js\\_rc.55.16947](https://doi.org/10.2458/azu_js_rc.55.16947).
- Resig, J.M., 1960, Foraminiferal ecology around ocean outfalls off southern California, in Pearson, P.A., ed., *Waste Disposal in the Marine Environment*: London, Pergamon Press, p. 104–121, <https://doi.org/10.1016/B978-0-08-009534-9.50014-4>.
- Ritter, W.E., 1901, Some observations bearing on the probable subsidence during recent geological times of the island of Santa Catalina off the coast of southern California: *Science*, v. 14, p. 575–577, <https://doi.org/10.1126/science.14.354.575>.
- Rockwell, T.K., Keller, E.A., and Dembroff, G.R., 1988, Quaternary rate of folding of the Ventura Avenue anticline, western Transverse Ranges, southern California: *Geological Society of America Bulletin*, v. 100, no. 6, p. 850–858, [https://doi.org/10.1130/0016-7606\(1988\)100<0850:QROFOT>2.3.CO;2](https://doi.org/10.1130/0016-7606(1988)100<0850:QROFOT>2.3.CO;2).
- Rohling, E.J., Fenton, M., Jorissen, F.J., Bertrand, P., Ganssen, G., and Cauter, J.P., 1998, Magnitudes of sea-level lowstands of the past 500,000 years: *Nature*, v. 394, p. 162–165, <https://doi.org/10.1038/28134>.
- Samaras, W.F., and Gellera, J.A., 1979, Recognition of Quaternary wave-formed marine terraces on Santa Catalina Island: *Bulletin of the Southern California Academy of Sciences*, v. 78, p. 20–31.
- Sandwell, D.T., 2001, Flexure of the lithosphere: Lecture notes, <http://topex.ucsd.edu/geodynamics/12flexure.pdf>.
- Sautter, L.R., and Thunell, R.C., 1991, Planktonic foraminiferal response to upwelling and seasonal hydrographic conditions; sediment trap results from San Pedro Basin, southern California Bight: *Journal of Foraminiferal Research*, v. 21, p. 347–363, <https://doi.org/10.2113/gsjfr.21.4.347>.
- Schumann, R.R., Minor, S.A., Muhs, D.R., Groves, L.T., and McGeehin, J.P., 2012, Tectonic influences on the preservation of marine terraces: Old and new evidence from Santa Catalina Island, California: *Geomorphology*, v. 179, p. 208–224, <https://doi.org/10.1016/j.geomorph.2012.08.012>.
- Shaw, J.H., and Suppe, J., 1994, Active faulting and growth folding in the eastern Santa Barbara Channel, Cali-

- fornia: Geological Society of America Bulletin, v. 106, p. 607–626, [https://doi.org/10.1130/0016-7606\(1994\)106<0607:AFAGFI>2.3.CO;2](https://doi.org/10.1130/0016-7606(1994)106<0607:AFAGFI>2.3.CO;2).
- Sheffels, B., and McNutt, M., 1986, Role of subsurface loads and regional compensation in the isostatic balance of the Transverse Ranges, California: Evidence for intracontinental subduction: *Journal of Geophysical Research*, v. 91, p. 6419–6431, <https://doi.org/10.1029/JB091iB06p06419>.
- Shepard, F.P., Grant, U.S., and Dietz, R.S., 1939, The emergence of (Santa) Catalina Island: *American Journal of Science*, v. 237, p. 651–655, <https://doi.org/10.2475/ajs.237.9.651>.
- Smith, W.S.T., 1933, Marine terraces on Santa Catalina Island: *American Journal of Science*, v. 25, p. 123–136, <https://doi.org/10.2475/ajs.s5-25.146.123>.
- Spratt, R.M., and Lisiecki, L.E., 2015, A late Pleistocene sea-level stack: *Climate of the Past Discussions*, v. 11, p. 3699–3728, <https://doi.org/10.5194/cpd-11-3699-2015>.
- Steinen, R.P., Harrison, R.S., and Matthews, R.K., 1973, Eustatic low stand of sea level between 125,000 and 105,000 B.P.: Evidence from the subsurface of Barbados, West Indies: *Geological Society of America Bulletin*, v. 84, p. 63–70, [https://doi.org/10.1130/0016-7606\(1973\)84<63:ELSOSL>2.0.CO;2](https://doi.org/10.1130/0016-7606(1973)84<63:ELSOSL>2.0.CO;2).
- Stock, J.M., and Hodges, K.V., 1989, Pre-Pliocene extension around the Gulf of California and the transfer of Baja California to the Pacific plate: *Tectonics*, v. 8, no. 1, p. 99–115, <https://doi.org/10.1029/TC008i001p00099>.
- Stuart, C.J., 1979, Lithofacies and origin of the San Onofre Breccia, coastal southern California, in Stuart, C.J., ed., *A Guidebook to Miocene Lithofacies and Depositional Environments, Coastal Southern California and Northwestern Baja California*: Los Angeles, California, Pacific Section, Society of Economic Paleontologists and Mineralogists (SEPM), p. 25–42.
- Stuiver, M., and Reimer, P.J., 1993, Extended <sup>14</sup>C database and revised CALIB radiocarbon calibration program: *Radiocarbon*, v. 35, p. 215–230, <https://doi.org/10.1017/S0033822200013904>.
- Stuiver, M., Reimer, P.J., and Reimer, R.W., 2005, CALIB 7.10: <http://calib.qub.ac.uk/calib> (accessed 20 December 2017).
- Turcotte, D.L. and McAdoo, D.C., 1979, Thermal subsidence and petroleum generation in the southwestern block of the Los Angeles Basin, California: *Journal of Geophysical Research*, v. 84, no. B7, p. 3460–3464, <https://doi.org/10.1029/JB084iB07p03460>.
- Uchio, T., 1960, Ecology of Living Benthonic Foraminifera from the San Diego, California, Area: *Cushman Foundation for Foraminiferal Research Special Publication*, 72 p.
- U.S. Department of Agriculture, Natural Resources Conservation Service (USDA), 2008, Soil Survey of Santa Catalina Island, California: [https://www.nrcs.usda.gov/Internet/FSE\\_DOCUMENTS/16/nrcs143\\_017732.pdf](https://www.nrcs.usda.gov/Internet/FSE_DOCUMENTS/16/nrcs143_017732.pdf) (accessed 16 June 2016).
- Vedder, J.G., Howell, D.G., and Forman, J.A., 1979, Miocene strata and their relation to other rocks Santa Catalina Island, CA, in Armentrout, J.M., Cole, M.R., and TerBest, H., Jr., eds., *Cenozoic Paleogeography of the Western United States*: Los Angeles, California, Pacific Section, Society of Economic Paleontologists and Mineralogists (SEPM), *Pacific Coast Paleogeography Symposium 3*, p. 239–256.
- Vedder, J.G., Greene, H.G., Clarke, S.H., and Kennedy, M.P., 1986, *Geologic Map of the Mid-Southern California Continental Margin*: California Division of Mines and Geology California Continental Margin Map Series, Area 2 of 7, sheet 1 of 4, scale 1:250,000.
- Wade, B.S., Pearson, P.N., Berggren, W.A., and Pälike, H., 2011, Review and revision of Cenozoic tropical planktonic foraminiferal biostratigraphy and calibration to the geomagnetic polarity and astronomical time scale: *Earth-Science Reviews*, v. 104, p. 111–142, <https://doi.org/10.1016/j.earscirev.2010.09.003>.
- Walton, W.R., 1955, Ecology of living benthonic foraminifera, Todos Santos Bay, Baja California: *Journal of Paleontology*, v. 29, p. 952–1018.
- Williams, E.F., Castillo, C.M., Klemperer, S.L., Raineault, N.A., and Gee, L., 2018, Sycamore Knoll: A wave-planed pop-up structure in a sinistral-oblique thrust system, Southern California Continental Borderland, in Raineault, N., Bell, K., and Girguis, P., eds., *Results of Telepresence-Enabled Oceanographic Exploration: Deep Sea Research Part II: Topical Studies in Oceanography*, v. 150, p. 132–145, <https://doi.org/10.1016/j.dsr2.2018.03.002>.
- Woodford, A.O., 1925, The San Onofre Breccia, its nature and origin: *University of California Publications in Geological Sciences*, v. 15, p. 159–280.
- Zalesny, E.R., 1959, Foraminiferal ecology of Santa Monica Bay, California: *Micropaleontology*, v. 5, p. 101–126, <https://doi.org/10.2307/1484158>.

SCIENCE EDITOR: DAVID SCHOFIELD  
 ASSOCIATE EDITOR: DANIEL CLAY KELLY  
 MANUSCRIPT RECEIVED 4 JANUARY 2017  
 REVISED MANUSCRIPT RECEIVED 4 MAY 2018  
 MANUSCRIPT ACCEPTED 27 JULY 2018  
 Printed in the USA